



UNIL | Université de Lausanne

Unicentre
CH-1015 Lausanne
<http://serval.unil.ch>

Year: 2024

The Role of mtDNA in Senescence and Prostate Cancer Immune Response Regulation

Lai Ping

Lai Ping, 2024, The Role of mtDNA in Senescence and Prostate Cancer Immune Response Regulation

Originally published at : Thesis, University of Lausanne

Posted at the University of Lausanne Open Archive <http://serval.unil.ch>

Document URN : [urn:nbn:ch:serval-BIB_DC897A84135C4](https://nbn-resolving.org/urn:nbn:ch:serval-BIB_DC897A84135C4)

Droits d'auteur

L'Université de Lausanne attire expressément l'attention des utilisateurs sur le fait que tous les documents publiés dans l'Archive SERVAL sont protégés par le droit d'auteur, conformément à la loi fédérale sur le droit d'auteur et les droits voisins (LDA). A ce titre, il est indispensable d'obtenir le consentement préalable de l'auteur et/ou de l'éditeur avant toute utilisation d'une oeuvre ou d'une partie d'une oeuvre ne relevant pas d'une utilisation à des fins personnelles au sens de la LDA (art. 19, al. 1 lettre a). A défaut, tout contrevenant s'expose aux sanctions prévues par cette loi. Nous déclinons toute responsabilité en la matière.

Copyright

The University of Lausanne expressly draws the attention of users to the fact that all documents published in the SERVAL Archive are protected by copyright in accordance with federal law on copyright and similar rights (LDA). Accordingly it is indispensable to obtain prior consent from the author and/or publisher before any use of a work or part of a work for purposes other than personal use within the meaning of LDA (art. 19, para. 1 letter a). Failure to do so will expose offenders to the sanctions laid down by this law. We accept no liability in this respect.



UNIL | Université de Lausanne

Faculté de biologie
et de médecine

**Institut/Section/Département de Institute of Oncology Research
(IOR, Bellinzona)**

The role of mtDNA in senescence and prostate cancer immune response regulation

Thèse de doctorat ès sciences de la vie (PhD)

présentée à la

Faculté de biologie et de médecine
de l'Université de Lausanne

par

Ping Lai

Master en biochimie et biologie moléculaire, Université de Chongqing, Chine.

Jury

Prof. Werner Held, Président
Prof. Romero Pedro, Directeur de thèse
Prof. Andrea Alimonti, Co-directeur de thèse (Institute of Oncology Research, IOR,
Bellinzona)
Prof. Tatiana Petrova, Experte
Prof. Fabio Grassi, Expert

Lausanne
(2024)

Imprimatur

Vu le rapport présenté par le jury d'examen, composé de

Président·e	Monsieur	Prof.	Werner	Held
Directeur·trice de thèse	Monsieur	Prof.	Pedro	Romero
Co-directeur·trice	Monsieur	Prof.	Andrea	Alimonti
Expert·e-s	Madame	Prof.	Tatiana	Petrova
	Monsieur	Prof.	Fabio	Grassi

le Conseil de Faculté autorise l'impression de la thèse de

Ping Lai

Master in Biochemistry and Molecular Biology, Chongqing University, Chine

intitulée

**The role of mtDNA in senescence and
prostate cancer immune response regulation**

Lausanne, le 5 mars 2024

pour le Doyen
de la Faculté de biologie et de médecine



Prof. Werner Held

Acknowledgment

I am profoundly grateful to my family for their unwavering support and encouragement throughout the duration of my thesis. Despite the challenges posed by geographical distance and the constraints of the COVID-19 pandemic, their steadfast belief in me served as a constant source of motivation, reminding me of the importance of perseverance and determination in the face of adversity.

I extend my most profound appreciation to my esteemed PI, Andrea Alimonti, whose guidance and mentorship have been instrumental in shaping my academic journey. I am grateful for the opportunities provided and the invaluable lessons learned along the way. His belief in my potential has inspired me to strive for excellence in all aspects of my work.

To my dedicated colleagues, who have become like family to me over the course of these five and half years, I extend my heartfelt gratitude. Their camaraderie, support, and shared passion for our research endeavors have made every challenge surmountable and every success all the more rewarding. I am truly fortunate to have had the opportunity to collaborate and grow alongside such talented individuals.

I would also like to express my sincere appreciation to my cherished friends, whose unwavering support and encouragement have been a constant source of strength and inspiration. Despite the miles that may have separated us, their enduring friendship has remained a beacon of light during this journey.

To all those whose guidance, support, and friendship have contributed to my personal and academic growth, I offer my deepest gratitude. Their collective impact has been immeasurable, and I am forever indebted to each of them for helping me reach this significant milestone in my academic career.

Summary

DNA is a potent damage-associated molecular pattern (DAMP) signaling that, once in the extracellular space, triggers the activation of the innate immune system. Indeed, several studies demonstrated that there is cytosolic accumulation of nuclear genome-derived DNA in senescent cells. Mitochondrial dysfunction is a crucial feature of senescence, a critical biological determinant of aging and tumorigenesis. Mitochondrial DNA (mtDNA) can be released from mitochondria and promote inflammation as a cell stress response. A recent report proposes that senescent cells induced by sub-lethal apoptotic stress release mtDNA through BAX/BAK macropores that promote SASP. However, all these studies focused on the effect of cytosolic DNA when the senescence has been established. It remains elusive whether mtDNA is released during the initial stage of senescence induction and how it contributes to senescence. Moreover, mtDNA has been shown to be biologically active as a DAMP, and its extracellular release can directly trigger innate immune response.

Here, by using three different senescent models, we find that senescent cells release mtDNA to both the cytosol and the extracellular space. This process occurs even in the initial stage of senescence induction and precedes that of nuclear DNA, resulting in the activation of the cGAS/STING pathway and the establishment of cellular senescence. Intriguingly, by exploiting co-culture and in vivo cross-species experiments, we show that extracellular mtDNA released by senescent tumor cells is packaged in extracellular vesicles (EVs) and is specifically captured by polymorphonuclear myeloid-derived suppressor cells (PMN-MDSCs) in the tumor microenvironment. Mechanistically, PMN-MDSCs uptake mtDNA leads to enhanced immunosuppressive ability through cGAS-STING-NF- κ B activation. Pharmacological inhibition of mtDNA released from senescent tumor cells blocks the PMN-MDSCs immunosuppressive activity, improving the efficacy of therapy-induced senescence (TIS) in cancer. These results reveal the crucial role of mtDNA in initiating cellular senescence and immunosuppression independently of the SASP. Thus, targeting the mtDNA release-mediated pathway may hold promise to reprogram the immune suppressive microenvironment in patients treated with chemotherapy.

Résumé

L'ADN est un puissant signal moléculaire associé à des dommages qui, une fois dans l'espace extracellulaire, déclenche l'activation du système immunitaire inné. En effet, plusieurs études ont montré que de l'ADN génomique nucléaire s'accumule dans le cytoplasme des cellules sénescents. Le dysfonctionnement mitochondrial est une caractéristique majeure de la sénescence cellulaire qui est un mécanisme biologique clé du vieillissement et de la tumorigenèse. L'ADN mitochondrial (ADNmt) peut être libéré des mitochondries et favoriser l'inflammation en tant que réponse au stress cellulaire. Une récente étude a proposé que des cellules sénescents induites par un stress apoptotique subléthal pouvaient libérer de l'ADNmt par l'intermédiaire du macropore BAX/BAK, et ainsi favoriser le phénotype sécrétoire associé à la sénescence (PSAS). Cependant, toutes les études précédemment mentionnées se sont uniquement concentrées sur l'effet de l'ADN cytosolique lorsque la sénescence avait été préalablement établie. À ce jour, il n'a pas encore été clarifié si l'ADNmt est libéré au cours de la phase initiale de l'induction de la sénescence et comment ce dernier pourrait contribuer à l'établissement de la sénescence. De plus, il a été démontré que l'ADNmt est biologiquement actif en tant que motif moléculaire associé aux dommages (DAMP) et que sa libération extracellulaire pouvait directement déclencher une réponse immunitaire innée.

Dans notre étude, en utilisant trois différents modèles de sénescence, nous avons démontré que les cellules sénescents libèrent de l'ADNmt à la fois dans le cytosol et dans l'espace extracellulaire. Ce processus se produit au stade initial de l'induction de la sénescence et précède la libération de l'ADN nucléaire, et entraîne l'activation de la voie cGAS/STING et ainsi l'établissement de la sénescence cellulaire. Curieusement, en réalisant des expériences de coculture et de croisement d'espèces *in vivo*, nous avons montré que l'ADNmt extracellulaire, libéré par les cellules tumorales sénescents, se trouvait incorporé dans des vésicules extracellulaires (VE) et était spécifiquement capturé par les cellules suppressives polymorphonucléaires dérivées des myéloïdes (PMN-MDSC) dans le microenvironnement tumoral (TME). L'incorporation de l'ADNmt par les PMN-MDSC permet l'amélioration de la capacité immunosuppressive par l'activation de cGAS-STING-NF- κ B.

L'inhibition pharmacologique de l'ADNmt libéré par les cellules tumorales sénescents bloque l'activité immunosuppressive des PMN-MDSC, améliorant ainsi l'efficacité de la sénescence induite par la thérapie (TIS) dans le cancer. Ces résultats révèlent donc le rôle crucial de l'ADNmt dans le déclenchement de la sénescence cellulaire et de l'immunosuppression indépendamment du PSAS. Ainsi, le ciblage de la voie de libération de l'ADNmt pourrait s'avérer prometteur pour reprogrammer le microenvironnement immunosuppresseur chez les patients traités par chimiothérapie.

List of Abbreviation

AIF	Apoptosis Inducing Factor
AMPK	5' Adenosine Monophosphate-activated Protein Kinase
BMDC	Bone Marrow-differentiated Dendritic cells
BM-MDSC	Bone Marrow-differentiated MDSC
BMDM	Bone Marrow-differentiated Macrophage cells
CCF	Cytoplasmic Chromatin Fragments
cGAS	Cyclic GMP-AMP synthase
CM-H2DCFDA	Chloromethyl 2',7'-Dichlorodihydrofluorescein diacetate
CsA	Cyclosporin A
DAMPs	Danger-associated Molecular Patterns
DAPI	4',6-diamidino-2-phenylindole
DDR	DNA damage response
Dendritic Cell	DC
Drp1	Dynamin-related protein 1
EndoG	Endonuclease G
EVs	Extracellular Vesicles
MAPK	Mitogen-activated Protein Kinases
MDSC	Myeloid-derived Suppressor Cells
Mfn1/2	Mitofusin 1 and 2
MiDAS	Mitochondrial Dysfunction-Associated Senescence
Mito-TEMPO	Mitochondria-targeted antioxidant
MOMP	Mitochondrial Outer Membrane Permeabilization
NAD ⁺	Nicotinamide Adenine Dinucleotide
NADH	Nicotinamide Adenine Dinucleotide Hydrogen (H)
NK	Natural Killer cells
OIS	Oncogene-induced Senescence
OPA1	OPA1 mitochondrial dynamin like GTPase
OXPPOS	Oxidative Phosphorylation
PCa	Prostate Cancer
PMN-MDSCs	Polymorphonuclear Myeloid-derived Suppressor Cells
PICS	<i>Pten</i> loss-induced Senescence

PTEN	Phosphatase and tensin homolog
PINK1	PTEN-induced putative kinase 1
ROS	Reactive Oxygen Species
SASP	Senescence-associated Secretory Phenotype
STING	Stimulator of Interferon Genes
TIS	Therapy-induced Senescence
TME	Tumor Microenvironment
TFAM	Mitochondrial Transcription Factor A
TLR9	Toll-like Receptor 9
VBIT-4	An inhibitor of VDAC1
VDAC1	Voltage-dependent Anion Channel 1
VDAC2	Voltage-dependent Anion Channel 2
VEGF	Vascular Endothelial Growth Factor

Table of Contents

Acknowledgment.....	i
Summary.....	ii
Résumé.....	iii
List of Abbreviation.....	v
Table of Contents.....	i
List of figures and Tables.....	i
1. Introduction.....	1
1.1 Senescence in Cancer.....	1
1.2 Senescence-associated Secretory Phenotype (SASP).....	2
1.3 Senescence and Mitochondrial Dysfunction.....	4
1.4 Cytosolic DNA Accumulation in Senescence.....	7
1.5 Research Aims.....	8
2. Methods and materials.....	9
2.1 Mice.....	9
2.2 Cell lines.....	9
2.3 Generation of <i>Pten</i> KO MEFs and <i>HRasV12</i> MEFs.....	9
2.4 Generation of <i>shEndog</i> and <i>shVdac1</i> , 2 MEFs.....	10
2.5 Differentiation of BM-MDSCs, BMDC, and BMDM in vitro.....	10
2.6 In vitro T cell suppression assay.....	10
2.7 Senescence associated β -galactosidase (SA- β -gal) assay.....	11
2.8 Immunohistochemistry (IHC) and Immunofluorescence (IF).....	11
2.9 Characterization of the immune tumor microenvironment.....	12
2.10 Quantitative real-time PCR (RT-qPCR).....	12
2.11 Cytosolic mitochondrial DNA (mtDNA) extraction and quantification.....	13
2.12 Western blot.....	14
2.13 Cell fractionation.....	15
2.14 cGAS Immunoprecipitation-PCR.....	16
2.15 Co-culture Experiment.....	16
2.16 DNA dot blot.....	16
2.17 Extracellular vesicles isolation, purification, and characterization.....	17

2.18 Extraction and quantification of plasma cfDNA	17
2.19 Gene Expression Profiling	18
2.20 Statistical Analysis	19
3. Results	20
3.1 Senescent cells release mtDNA to cytosol and extracellular space.....	20
3.2 mtDNA is required for senescence induction and activate cGAS-STING pathway to regulate SASP	22
3.3 Senescent tumor cells release mtDNA to cytosol and extracellular space	24
3.4 Senescent tumor cells released mtDNA is uptaken by PMN-MDSCs	26
3.5 Senescent tumor cells released mtDNA is packaged in extracellular vesicles (EVs)	28
3.6 MtDNA released by senescent tumor cells enhances the immune suppressive function of MDSCs	31
3.7 MtDNA enhances the immune suppressive function of MDSCs by activating the cGAS- STING-NF- κ B pathway	33
3.8 mtROS and EndoG regulate mtDNA release in senescent cells.....	36
3.9 Senescent cells release mtDNA through VDAC.....	40
3.10 Blockage of mtDNA release improves TIS efficacy	43
Discussion	47
Reference.....	52

List of Figures and Tables

Figure 1: Establishment of senescent models in MEFs.

Figure 2: Senescent MEFs release fragmented mtDNA to cytosol and culture media.

Figure 3: mtDNA is essential for senescence induction.

Figure 4: Cytosolic mtDNA activates the cGAS-STING pathway to regulate SASP.

Figure 5: Senescent tumor cells also release mtDNA to cytosol and culture media.

Figure 6: mtDNA is essential for senescence induction in tumor cells.

Figure 7: Senescent cells released mtDNA, which is uptaken by PMN-MDSC.

Figure 8: Senescent cells released mtDNA is packed in EVs.

Figure 9: PMN-MDSCs uptake senescent cells derived mtDNA through EVs.

Figure 10: Senescent cells derived mtDNA enhances the immune suppressive function of MDSCs.

Figure 11: Senescent cells derived mtDNA activates the cGAS-STING pathway in MDSCs.

Figure 12: MtDNA enhances the immune suppressive function of MDSCs by activating the STING-NF- κ B pathway.

Figure 13: mtROS induces mtDNA release in senescent cells.

Figure 14: Nuclear translocation of EndoG is required for mtDNA release.

Figure 15: EndoG deficiency promotes mtDNA release and enhances senescence.

Figure 16: Cytosolic mtDNA releases in senescent cells occur through VDAC.

Figure 17: VDAC1 inhibitor blocks mtDNA release and senescence induction.

Figure 18: VBIT-4 treatment blocks mtDNA release, enhancing the efficacy of TIS.

Figure 19: VBIT-4 treatment inhibits PMN-MDSC immunosuppressive function *in vivo*.

Table 1: Primer sequence used in this study.

1. Introduction

1.1 Senescence in Cancer

Cellular senescence, a stable form of cell growth arrest, can be induced by a range of stimuli, including DNA damage, cellular stress, telomere shortening, and the activation of oncogenes. Cellular senescence regulates physiological and homeostatic processes but can also be a pathological process that contributes to aging, age-related diseases, and cancer development^{1,2}. In cancer, senescence is generally regarded as a physiological tumor suppressive process which inhibits cancer cell proliferation and suppresses oncogenic progression. This may be mediated by the DNA damage response or via crucial oncogenes. Oncogenic signaling activation in mammalian cells, including Ras, Cyclin E, Raf, and E2F3 expression, results in a robust and sustained proliferative stress and senescence induction that limits tumor growth³⁻⁵, which is termed oncogene-induced senescence (OIS). It has since been established that approximately 50 oncogenes have the capacity to induce senescence⁶. Accordingly, the mechanisms and pathways mediating OIS are complex and incompletely elucidated. They involve the activation of both the RB and p53 pathways³, the inhibition of mitogenic signaling, and also the contribution of inflammatory signaling activation⁷. OIS was initially thought to be a barrier to malignant transformation because of cell proliferation suppression. However, some studies lately also shown that OIS can promote the initiation and development of cancer². The diverse effects of OIS occur through different combinations of downstream effectors as well as the interplay of senescent cells and the microenvironment⁸.

Likewise, the loss of tumor suppressor genes, such as PTEN, can also induce senescence in primary prostate epithelium, referred to as PTEN-loss-induced cellular senescence (PICS). It has been demonstrated that PTEN is a pivotal determinant that dictates premature senescent and apoptotic phenotypes in glioma cells following ionizing radiation (IR) exposure; PTEN-

mutant cells underwent premature senescence while cancer cells expressing PTEN underwent apoptosis⁹. Inactivation of PTEN has the potential for pro-senescence cancer therapy *in vitro* and in mice^{10,11}. In addition, the inactivation of PTEN resulted in p53-mediated senescence and suppression of tumorigenesis in mice¹². It has been proposed that a loss of one of the vital senescence effectors, such as the tumor suppressors, p16^{INKA4} or p53, may be mechanism whereby the failure of senescence occurs⁵. Some mechanisms to evade senescence are, therefore, a key feature of malignant progression from pre-malignant to invasive disease.

Despite the ability of malignant tumors to evade senescence, cellular senescence is also a key effector mechanism of many types of anti-cancer therapies^{13,14}. Conventional anticancer therapeutics, such as chemotherapy, radiotherapy, and endocrine therapies, can force the cancer cells to enter a senescent state, which is termed therapy-induced senescence (TIS)^{2,5}. The mechanisms that force tumor cells into senescence by irradiation are generally linked to DNA damage enhancement¹⁵. Primary murine lymphomas have been shown to respond to chemotherapeutic treatment with cyclophosphamide by engaging a senescence program controlled by p16^{INK4a} and p53¹⁶. Several targeted therapies that inhibit CDKs, NOTCH, CK2, MDM2, JAK2, and SKIP2 can also promote growth arrest and senescence in tumors of different genetic backgrounds^{17,18}. Intriguingly, some clinically available compounds can also block senescence induced by chemotherapy or oncogenic stress, limiting the outcome of the treatment. For instance, the CDK4/6 inhibitors, palbociclib, and abemaciclib, induce senescence in preclinical models of breast cancer and can reduce tumor volume via activation of interferon-mediated immunosurveillance¹⁹.

1.2 Senescence-associated Secretory Phenotype (SASP)

Except for the direct anti-tumor effect due to the tumor cell proliferation arrest, senescent cells may also evoke an anti-tumor response via molecules released by senescent cells that may

stimulate an immune response ²⁰. Indeed, senescent cells remain metabolically active and release in the tumor microenvironment a number of secreted factors, which range from proinflammatory cytokines and chemokines to growth factors and proteases, termed senescence-associated secretory phenotype (SASP) ²¹. The SASP can reinforce the senescence program and influence the tumor microenvironment, impacting the stroma and the tumor immune cells ²¹. For instance, IL8 and IL6, two prominent cytokines of SASP, are needed for the maintenance of senescence ^{22,23}. Inhibition of IL6 or IL6 receptors promotes senescence evasion in OIS ²². Similarly, inhibition of CXCR2, which prevents the binding of IL8, also promotes senescence bypass in OIS ²². In addition, SASP factors can also induce senescence of surrounding cells in a paracrine manner and impact tumor suppression and senescence *in vivo* ^{24,25}. Moreover, the SASP is composed of a number of chemokines and cytokines that can promote the recruitment and activation of both innate and adaptive immune cells, including M1-like macrophages, natural killer (NK) cells, and T-helper 1 (Th1) lymphocytes ^{26,27}. Such immune infiltrates can restrain tumor progression by mediating the clearance of senescent tumor cells, so-called “senescence surveillance” ^{20,25,28}.

However, accumulating evidence shows that the SASP of senescent cells may have a tumor-suppressive function and trigger immune activation or promote tumor growth and inflammation that works as a double-edged sword in cancer progression^{21,29}. The most pro-tumorigenic effect of the SASP is to promote the proliferation of epithelial cells, and the secreted array of factors can reprogram the microenvironment to promote cell migration and invasion ²¹. Initially, it was reported that senescent stromal cells release vascular endothelial growth factor (VEGF) to stimulate angiogenesis, which leads to a tumor-promoting effect in breast cancer ³⁰. Senescent fibroblasts from the human prostate gland have also been shown to create a local tissue microenvironment via a consistent program of gene expression that leads to hyperproliferation of prostate epithelial cells and the progression of prostate neoplasia ³¹. Another pro-tumorigenic

effect of senescent cells mediated by SASP is the recruitment of myeloid-derived suppressor cells (MDSCs) and immature myeloid cells to the tumor, creating an immunosuppressive microenvironment that drives increased tumorigenesis³²⁻³⁴. These myeloid cells antagonize the establishment of senescence in cancer cells by blocking IL-1 α signaling and also block immune surveillance by inhibiting CD8⁺ T cells (mediated by IL-6³²) and NK cells (mediated by the chemokine CCL2³⁴). There is also evidence that “immune senescence”, associated with the aging of the immune system in older age, may contribute to the failure of immune surveillance and contribute to cancer development³⁵. Recent findings demonstrate that soluble factors from tumors can induce human T cells to develop a senescent-like phenotype that is also associated with the suppression of responder T cell proliferation³⁶.

However, the pro-tumorigenic and anti-tumorigenic effects of senescent cancer cells are likely mediated by a complex interplay between multiple SASP factors and the immune microenvironment. Recently, the elimination of senescent cells has emerged as a promising strategy to arrest tumor growth and inhibit metastase formation^{25,37}. Therefore, understanding the exact mechanisms regulating senescence and the SASP is very important from the medical perspective.

1.3 Senescence and Mitochondrial Dysfunction

Emerging evidence has pinpointed mitochondria as one of the key modulators in the development of senescence. Data suggest that mitochondrial dysfunction is a general feature of cellular senescence³⁸. In senescent cells, mitochondria are identified as dysfunctional, as they show an increase in mitochondrial mass, decreased mitochondrial membrane potential, increased ROS levels, and activation of AMPK³⁸⁻⁴². Increased mitochondrial mass and PGC-1 α , NRF1 and/or NRF2, TFAM induction were associated with replicative, oxidative stress-induced senescence and oncogene-induced senescence^{39,43}, suggesting a role for mitochondrial

biogenesis in promoting mitochondrial mass increase and premature induction of senescence. However, the increase in mitochondrial mass is complemented by changes in mitochondrial fission and fusion processes (known as mitochondrial dynamics), and impaired mitophagy process. Mitochondrial fusion allows the exchange of damaged mitochondria with healthy ones to rearrange the mitochondrial component and repair the mitochondrial function and involves fusion proteins such as Mitofusin 1 and 2 (Mfn1/2) and optic atrophy protein 1 (OPA1). Mitochondrial fission can produce new mitochondria by recruitment of Drp1 protein to the surface of mitochondria by receptors like FIS1, Mff, and mitochondrial dynamics proteins such as MiD49 and MiD51. Perturbations in mitochondrial dynamics and mitochondrial elongation have been associated with cellular senescence and induction of senescence-associated pathways^{44,45}. Another mechanism that maintains mitochondrial homeostasis and healthy function is mitophagy. With mitochondria depolarization, the PTEN-induced putative kinase 1 (PINK1) accumulates on the outer mitochondrial membrane, where it recruits and activates the E3 ligase Parkin and other autophagic receptors to mitochondria to induce mitophagy, which can specifically degrade dysfunctional or damaged mitochondria and control both the quality and quantity of mitochondria⁴². It has been published that senescent cells have impaired mitophagy, and effects in mitophagy may play a role in the induction of cellular senescence⁴⁶. For example, a study revealed that excessive S-Nitrosylation of Parkin, resulting in decreased fission, was responsible for altered mitophagy in senescence⁴⁷. Mechanistically, during senescence, cytosolic accumulated p53 protein binds to Parkin in the cytosol, leading to the inhibition of Parkin translocate to the mitochondria. This process has been shown to maintain or reinforce the senescence phenotype⁴⁸⁻⁵⁰.

In addition to dramatic changes in morphology and dynamics, the mitochondria in senescent cells also show functional alterations. Cells undergoing senescence display altered mitochondrial metabolite homeostasis, such as increased mitochondrial ROS production,

decreased NAD^+/NADH ratios⁵¹⁻⁵³, increased AMP/ATP and ADP/ATP ratios⁵⁴, as well as increased lipids accumulation due to decreased fatty acid oxidation⁵⁵. Senescent cells contain dysfunctional mitochondria, and several studies indicate that the impaired mitochondria with inefficient OXPHOS produce excessive ROS^{39,56,57}. ROS has been shown to contribute to damage to several macromolecules, including proteins, lipids, and DNA⁷. In the context of cellular senescence, mitochondrial ROS has been shown to induce DNA damage, such as oxidized bases, single-strand breaks, double-strand breaks, and telomere shortening, activating p53 and pRb pathways and causing cell cycle arrest and senescence⁵⁸. It was also identified that low NAD^+/NADH levels provoke a cell cycle arrest, which was not caused by DNA damage but, in addition, drove p53 activation through AMPK (5' adenosine monophosphate-activated protein kinase), in turn, was shown to initiate the IL-1 arm of the SASP⁵¹. In general, cells with reduced NAD^+/NADH ratio display less efficiency in producing ATP, leading to a bioenergetic imbalance with an increase in AMP/ATP ratio⁵⁹. The elevated ADP/ATP and AMP/ATP ratios can activate AMPK, which in turn induces senescence by phosphorylating p53 and/or stabilizing p16^{INK4} mRNA⁵¹.

In fact, dysfunctional mitochondria can also drive the senescent phenotype. Wiley et al. show that mitochondrial defects cause a distinct senescence phenotype termed MiDAS (mitochondrial dysfunction-associated senescence), which has a specific secretome that is able to drive some of the aging phenotypes⁵¹. Damaged mitochondria have been implicated in the induction of the NLRP3 inflammasome through ROS and the release of mitochondrial DNA (mtDNA)^{60,61}. Also, dysfunctional mitochondria due to the histone-like mitochondrial transcription factor (TFAM) deficiency triggers a type I cytokine storm that induces senescence in several tissues³⁵. Interestingly, West and colleagues demonstrated that heterozygosity of TFAM caused disruption of mtDNA stability, which results in the release of mtDNA into the cytosol via an unknown mechanism⁶². Once in the cytoplasm, mtDNA elicits type I interferon

(IFN) production through the cGAS-STING pathway. Furthermore, pathogenic mtDNA has also been reported to be involved in cellular senescence. Nevertheless, the contribution of mitochondria to the development of the senescent phenotype, as well as the underlying mechanism driving mitochondrial dysfunction in aging and age-related diseases, require further elucidation, as this knowledge might contribute to the discovery of new targets for possible anti-aging interventions.

1.4 Cytosolic DNA Accumulation in Senescence

Recent studies have shed light on the accumulation of cytosolic nuclear DNA in the form of cytoplasmic chromatin fragments (CCF) in senescent cells. Once CCF enter the cytoplasm, they are sensed by the cyclic GMP-AMP synthase-stimulator of interferon genes (cGAS-STING) pathway that activates the SASP through NF- κ B⁶³⁻⁶⁶. Except for nuclear DNA, cells also contain high copy numbers of mitochondrial circular DNA (mtDNA) densely packaged into nucleoids, which is more susceptible to damage than nuclear DNA (nDNA)⁶⁷. In response to various stresses, such as apoptosis^{68,69}, viral infection^{70,71}, TFAM deficiency⁶², and oxidative stress⁶⁰, mtDNA is released in the cytosol, where it is recognized as a foreign danger to trigger inflammation by the cGAS-STING pathway^{62,72,73}. A recent report proposes that senescent cells induced by sub-lethal apoptotic stress release mtDNA through BAX/BAK macropores that promote SASP⁷⁴. However, all these studies focused on the effect of cytosolic DNA when the senescence has been established. It remains elusive whether mtDNA is released during the initial stage of senescence induction and how it contributes to the establishment of senescence.

Cellular mtDNA can also be released outside of the cell as circulating cell-free mtDNA (ccf-mtDNA). Elevated ccf-mtDNA levels are associated with tissue injury, inflammatory diseases, and cancer^{75,76}. As a damage-associated molecular pattern (DAMP) molecule, the circulating mtDNA can trigger inflammatory responses via different signaling axis, thereby contributing

to diverse pathological processes⁷⁷⁻⁸⁰. For instance, in injured tissues or sepsis, mtDNA is released to the extracellular space, can be detected in circulation, and directly causes inflammation by activation of TLR9 on neutrophils⁸¹ or red blood cells⁸², respectively. As recently demonstrated, the SASP of senescent tumor cells can cause immune suppression^{7,83,84} and tumor progression by recruiting PMN-MDSCs^{1,33,83}. While, whether mtDNA is released to TME from senescent tumor cells and is involved in the reprogramming of the surrounded environment independently by the SASP remains largely unexplored.

1.5 Research Aims

So far, mitochondria have been implicated as having an essential role in driving the pro-inflammatory features of senescence, although the underlying mechanisms responsible remain unknown. MtDNA has recently been reported released to the cytosol through BAX/BAK macropore to promote SASP in senescent cells, which is induced by sub-lethal apoptotic stress release mtDNA⁷⁴. However, whether mtDNA can also be released in non-lethal senescence models, such as replicative senescence, PIC, OIS, and TIS, which are more cancer-relevant, is still unknown. In addition, as a part of damage-associated molecular patterns (DAMPs), extracellular released mtDNA can trigger inflammatory responses. Whether senescent cells release mtDNA to the extracellular space and the function of the senescent cells-derived mtDNA in TME remains elucidated.

Therefore, the aims of this project are:

- 1) To elucidate the role of mtDNA during senescence induction;
- 2) To characterize the mechanism(s) by which mtDNA is released from the mitochondria into the cytosol in senescence;
- 3) To confirm whether senescent cells release mtDNA to extracellular space;
- 4) To explore the effect of extracellular mtDNA in the immune landscape of prostate cancer.

2. Methods and materials

2.1 Mice

All mice were maintained under specific pathogen-free conditions, and experiments were approved by the local ethical committee (“Dipartimento della Sanita’ e Socialita’, Esperimenti su animali” Canton Ticino), authorization number 34293. *Mb21d1^{-/-}* (cGAS knockout) mice were a gift from Prof. Andrea Ablasser (Ecole Polytechnique Fédérale de Lausanne, Switzerland). For allograft experiments, C57BL6/N were challenged with 2.5×10^6 TRAMP-C1 cells or RapidCap cells and then orally given Palbociclib (150 mg/Kg) three times and/or VBIT-4 (20 mg/Kg) five times per week when tumors were approximately 100 mm^3 . For the xenograft experiment, NRG mice were challenged with 2.5×10^6 PC3 cells and then orally given Palbociclib when tumors were about 100 mm^3 . Tumor volume and survival rate were analyzed, and mice were sacrificed when the tumor reached approximately 1000 mm^3 .

2.2 Cell lines

PC3 cells were purchased from ATCC and cultured in RPMI 1640 supplemented with 10% FBS and 1% P/S. TRAMP-C1 cells were purchased from ATCC; RapidCap is a kind gift from Prof. Lloyd C. Trotman (Cold Spring Harbor Laboratory) and cultured in DMEM supplemented with 10% FBS and 1% P/S. All cell lines were kept under controlled temperature (37°C) and CO_2 (5%) and tested negative for Mycoplasma.

2.3 Generation of *Pten* KO MEFs and *HRas*V12 MEFs

Primary Mouse Embryonic Fibroblasts (MEF) were obtained from pregnant *Pten^{lox/lox}* mice at 13.5 days post-coitum. Embryos were harvested, and the individual MEFs were cultured in DMEM containing 10% fetal bovine serum (FBS) and 1% Penicillin/Streptomycin (P/S). To prepare lentiviral particles, HEK-293T cells were transfected using JetPRIME® transfection reagents (JetPRIME®, Polyplus transfection, 114-07/712-60) as per the manufacturer’s

instructions. Primary MEFs were infected with retroviruses expressing either pWZL-Hygro (Addgene, #18750), pWZL-Hygro-CRE, or pWZL-Hygro-HRasV12 (Addgene, #18749) and selected with Hygromycin B (Invitrogen, 10687010) at a concentration of 50 µg/ml.

2.4 Generation of *shEndog* and *shVdac1, 2* MEFs

Primary MEFs were infected with shRNA using the mouse *Endog*-directed shRNA (Sigma), *Vdac1*, and *Vdac2* shRNA (Sigma). To prepare lentiviral particles, HEK-293T cells were transfected using JetPRIME transfection reagents as described above. MEFs cells were infected with the filtered lentiviral supernatant obtained from transfected HEK-293T cells and were subsequently selected using Puromycin (Sigma) at 3 µg/ml.

2.5 Differentiation of BM-MDSCs, BMDC, and BMDM in vitro

Mouse BM-MDSCs, BMDC, and BMDM were differentiated in vitro as previously described⁸⁵⁻⁸⁷. In brief, bone marrow cells were flushed from the legs of C57BL/6 with RPMI 1640 medium. The cell pellets were lysed with ACK buffer (Gibco, A1049201) to prepare the progenitors. To generate BMDM, the progenitors are resuspended in a complete DMEM medium containing 20 ng/ml M-CSF for 7 days. The medium is changed on day 3 and day 5. For BM-MDSCs, cells are resuspended in complete RPMI containing 40 ng/ml GM-CSF and 40 ng/ml IL-6 for 4 days. For BMDC, cells are resuspended in complete RPMI containing 20 ng/ml GM-CSF for 7 days.

2.6 In vitro T cell suppression assay

In vitro suppression assays were determined as previously described⁽⁸⁵⁾. In brief, the suppression assays were carried out in RPMI/10% FBS in 96-well U-bottom plates (Corning, NY). The naïve splenocytes were labeled with 2.5 µM CFSE (Thermo Scientific, C34554) and activated in vitro with anti-CD3/CD28 beads (Gibco, 11452D) according to the manufacturer's

instructions. BM-MDSCs were added to the culture. After three days, the proliferation of CFSE-labelled CD8⁺ T cells and CD4⁺ T cells was analyzed by BD FACS Canto I.

2.7 Senescence associated β -galactosidase (SA- β -gal) assay

For tissue-specific SA- β -gal assay, tumor samples were immediately frozen in OCT solution at -80°C , and sections of 8 μm were prepared. Senescence-associated SA- β -gal staining was performed using the Senescence β -Galactosidase Staining Kit (Cell Signaling Technology, 9860) according to the manufacturer's instructions. Counterstaining was performed using Eosin staining (Alcohol-based Diapath, C0352). SA- β -gal staining was performed using the Senescence β -Galactosidase Staining Kit (Cell Signalling Technology, Cat. No 9860) according to the manufacturer's instructions.

2.8 Immunohistochemistry (IHC) and Immunofluorescence (IF)

Tumor tissue samples were fixed in 10% neutral-buffered formalin (Thermo Scientific, Cat No. 5701) overnight and then washed thoroughly under running tap water, followed by processing using ethanol and embedded in paraffin according to standard protocols. Sections (5 μm) were prepared for antibody detection and hematoxylin and eosin staining. IHC tissue sections were processed as follows: de-paraffinized, unmasked, pre-staining, blockings, and secondary staining³⁷. Images were scanned with Aperio and opened with ImageScope v12.3.2.8013 (Leica Biosystem).

For in vitro immunofluorescence, all microscopy image cells were seeded on coverslips one day before fixation. After washing in PBS, cells were fixed with 4% paraformaldehyde for 20 min, permeabilized with 0.1% Triton X-100 in PBS for 15 min, blocked with PBS containing 10% FBS for 30 min, stained with primary antibodies at 4°C for overnight, and stained with secondary antibodies for 60 min at room temperature. Cells were washed with 0.1% PBS-Tween 20 between each step. Slides were covered with mounting media with DAPI (Invitrogen,

P36931), ready to be visualized under the fluorescent confocal microscope. Images were acquired on Leica TCS SP5 and merged using ImageJ software (NIH).

2.9 Characterization of the immune tumor microenvironment

Tumors were isolated and digested in collagenase D and *DNase* I for 30 min at 37 °C to obtain a single-cell suspension. The single cells were stained with Fixable viability stain (ThermoFisher Scientific) for 1 hour, and then CD16/ CD32 antibody was used to block the unspecific binding. Single-cell suspensions were stained with specific monoclonal antibodies (primary antibodies directly conjugated) to assess the phenotype and diluted 1:200. The antibodies used were: CD45 (clone 30-F11), Ly6C (clone HK1.4), Ly6G (clone 1A8), CD11b (clone M1/70), F4/80 (clone BM8), CD11c (clone N418), CD8 (clone 53-6.7), CD4 (clone GK1.5), CD3 (clone 17A2), B220 (clone RA3-6B2), CD19 (clone 1D3), CD49b (clone DX5). All antibodies were purchased from eBioscience, Biolegend, R&D, or BD. Samples were acquired on a BD FACSymphony (BD Biosciences). Data were analyzed using FlowJo software (TreeStar).

2.10 Quantitative real-time PCR (RT-qPCR)

Total RNA was extracted with TRIzol reagent (Ambion, 15596026) following the manufacturer's instructions. cDNA was obtained using an ImPROM II kit (Promega, A3800) according to the manufacturer's instructions. RT-qPCR was performed using Gotaq® qPCR Master Mix, Promega® (A6002) on Step One Real-Time PCR systems (Applied Biosystems). The target genes were normalized to the housekeeping gene (β -Actin) shown as $2^{-\Delta\Delta Ct}$. The used primers are listed in Table 1.

Table 1. Primer sequence used in this study.

Name	Forward	Reverse
Cdkn1a (p21)	TTCCCTCACAGGAGCAAAGT	CGGCGCAACTGCTCACT

Serpine1 (Pai1)	TTCAGCCCTTGCTTGCCTC- 3'	ACACTTTTACTCCGAAGTCGGT
18s rDNA	TAGAGGGACAAGTGGCGTTC	CGCTGAGCCAGTCAGTGT
Tert	CTAGCTCATGTGTCAAGACCCTCTT	GCCAGCACGTTTCTCTCGTT
Dloop	TCCTCCGTGAAACCAACAA	AGCGAGAAGAGGGGCATT
IL8	CTGGTCCATGCTCCTGCTG	GGACGGACGAAGATGCCTAG
Mmp3	TGGAGCTGATGCATAAGCCC	TGAAGCCACCAACATCAGGA
Endog	TTCCGCGAGGATGACTCTGT	CACCTGAGGCGCTACGTTG
ACTB	GATGCACAGTAGGTCTAAGTGGAG	CACTCAGGGCAGGTGAAACT
β-Actin	GGCTGTATTCCCCTCCATCG	CCAGTTGGTAACAATGCCATG
Ccl2	TTAAAAACCTGGATCGGAACCAA	GCATTAGCTTCAGATTTACGGGT
Cxcl10	CCAAGTGCTGCCGTCATTTTC	GGCTCGCAGGGATGATTTCAA
Ifi44	CTGATTACAAAAGAAGACATGACAGAC	AGGCAAAACCAAAGACTCCA
Ifit1	CAAGGCAGGTTTCTGAGGAG	GACCTGGTCACCATCAGCAT
Ifnb1	CCCTATGGAGATGACGGAGA	CCCAGTGCTGGAGAAATTGT
Isg15	CTAGAGCTAGAGCCTGCAG	AGTTAGTCACGGACACCAG
Vdac1	ACTAATGTGAATGACGGGACA	GCATTGACGTTCTTGCCAT
Cox1	GCCCCAGATATAGCATTCCC	GTTTCATCCTGTTCTGCTCC
IL1b	TGTAATGAAAGACGGCACACC	TCTTCTTTGGGTATTGCTTGG
Tnfa	CCCTCACACTCAGATCATCTTCT	GCTACGACGTGGGCTACAG
IL12	TACTAGAGAGACTTCTTCCACAACAAGAG	TCTGGTACATCTTCAAGTCCTCATAGA
S100A8	GTCCTCAGTTTGTGCAGAAATATAAA	GCCAGAAGCTCTGCTACTCC
IL6	TAGTCCTTCCTACCCCAATTTCC	TTGGTCCTTAGCCACTCCTTC
Nos2	GTTCTCAGCCCAACAATACAAGA	GTGGACGGGTCGATGTCAC
Arg1	CCACACTGACTCTTCCATTCTT	GATTATCGGAGCGCCTTTCT
hLINE1	TCACTCAAAGCCGCTCAACTAC	TCTGCCTTCATTTGCTTATGTACC
hND1	ATACCCATGGCCAACCTCCT	GGGCCTTTGCGTAGTTGTAT

2.11 Cytosolic mitochondrial DNA (mtDNA) extraction and quantification

1×10⁶ Cells were each divided into two equal aliquots, and one aliquot was resuspended in 300 µl of 50 µM NaOH and boiled at 95°C for 30 min to solubilize DNA. 30 µl of 1 M Tris-HCl pH 8 was added to neutralize the pH, and these extracts served as normalization controls for total mtDNA. The second equal aliquots were resuspended in roughly 300 µl buffer containing 150 mM NaCl, 50 mM HEPES pH 7.4, and 25 µg/ml digitonin (EMD Chemicals). The homogenates were incubated on a rotator for 10 min at room temperature, followed by centrifugation at 980g 4°C for 3 min three times to pellet intact cells. The cytosolic supernatants were then spun at 17000g for 20 min to pellet any remaining cellular debris. Quantitative PCR

was performed on both whole-cell extracts and cytosolic fractions using nuclear DNA primers (Tert) and mtDNA primers (Dloop3, Cox1), and the CT values obtained for mtDNA abundance for whole-cell extracts served as normalization controls for the mtDNA values obtained from the cytosolic fractions.

2.12 Western blot

Cells were lysed using 1×RIPA buffer (Cell signaling, 9806) containing protease and phosphatase inhibitors (Thermo Fisher, A32959) and then incubated on ice for 30 min. Samples were centrifuged at 13,000 g for 10 min. Protein concentration was determined by the BCA kit (Thermo Fisher, 23227). Equal amounts of proteins were subjected to SDS-polyacrylamide gel electrophoresis (SDS-PAGE), 10%, and transferred onto 0.45 μm PVDF membrane (Thermo Scientific, 88518). Membranes were blocked in 5% milk solution after protein transfer. Membranes were probed with the indicated antibodies overnight at 4 °C. The primary antibodies are: p16 (Abcam, ab211542), p21 (Abcam, ab107099), p27 (CST, 3698), HSP90 (CST, 4877), PTEN (CST, 9188), RAS (BD Transduction, 610001), p-HP1γ (CST, 2600), p-KAP1 (Thermo Fisher, A300-767A), p-γH2A.X (CST, 9718), GAPDH (CST, 5174), H4 (CST, 2592), p-STING (CST, 72971), STING (CST, 13647), p-TBK1 (CST, 5483), TBK1 (CST, 3504), STAT1 (CST, 9172), p-STAT1 (Y701) (CST, 9167), cGAS (CST, 31659), ENDOG (Sigma, SAB3500213), AIF (CST, 5318), VDAC1 (CST, 4661), VDAC2 (CST, 9412), Caspase-3 (CST, 9662), Cleaved Caspase-3 (CST, 9661), PARP (CST, 9542), p-Stat3 (CST, 9145), Stat3 (CST, 4904), NF-κB p65 (CST, 8242), Phospho-NF-κB p65 (CST, 3033), p-IRF-3 (CST, 4947), IRF-3 (CST, 4302), IκBα (CST, 4812), p-IκBα (CST, 2859). After washing with 1×PBST, the membranes were incubated with horseradish peroxidase-conjugated (HRP-linked) secondary antibodies anti-rat IgG (ThermoFisher Scientific, 31470, 1:5000), anti-rabbit IgG (Promega, W4011, 1:5000) or anti-mouse IgG (Promega, W4021, 1:5000) and developed using enhanced chemiluminescence (ECL) substrate (Thermo Scientific, 32106). Membranes were

exposed to the FusionSolo S imaging system (Vilber). Blots were semi-quantitatively analyzed by densitometry using ImageJ 1.52 v (National Institutes of Health).

2.13 Cell fractionation

A method was carried out for nuclei isolation as previously described with some modifications (Gagnon et al., 2014). Briefly, harvested cells were washed in ice-cold PBS and resuspended in hypotonic lysis buffer (10 mM Tris, pH 7.5, 10 mM NaCl, 3 mM MgCl₂, 0.3% NP-40, and 10% glycerol) in the presence of a protease/phosphatase inhibitor cocktail (Thermo Fisher Scientific). The suspension was incubated for 30 min on ice, passed ten times through a 28-gauge blunt-ended needle, and centrifuged at 400 g for 5 min at 4 °C. The nuclear pellet was washed three times with hypotonic lysis buffer and collected as a total nuclear fraction.

To isolate mitochondria-enriched cellular fractions, a crude mitochondrial fraction was first obtained, as described previously, with minor modifications⁸⁸. In brief, cells were washed with ice-cold PBS and suspended in chilled mitochondria isolation buffer (IBc) (10 mM Tris-MOPS, pH 7.4, 10 mM EGTA-Tris, 200 mM sucrose, and 5 mM MgCl₂) with a protease/phosphatase inhibitor cocktail. The cells were homogenized in IBc buffer using a Teflon pestle (about 50 strokes) and centrifuged at 500 g for 10 min at 4°C, followed by further centrifuging at 2,000 g for 10 min at 4°C to remove unbroken cells, cell debris, and nucleus. Then, the supernatant was collected and centrifuged at 7,500 g for 10 min at 4°C. The pellets containing mitochondria were washed twice with IBc buffer and saved the pellets as mitochondria fraction. Mitochondria-free cytosolic fraction was collected from the supernatant and centrifuged at 16,000 g for 15 min at 4°C. The supernatant was saved as a cytosolic fraction. Protein levels were determined using a Pierce BCA protein assay (Thermo Fisher Scientific), and each fraction was loaded for western blotting to confirm purity.

2.14 cGAS Immunoprecipitation-PCR

To pull down cytosolic endogenous cGAS, MEFs were fixed for 10 min in 4% PFA and quenched with 1 M Tris pH 7.4 for 5 min. Cytosolic fractions were isolated from the fixed cells following the previous procedures. Cytoplasm lysates were precleared with protein G magnetic beads (Invitrogen) and immunoprecipitated using anti-Rb cGAS (CST) or Rb Ig (CST) Protein G beads at 4°C overnight. Immunoprecipitates were washed five times with 50 mM Tris, 150 mM NaCl, 1 mM EDTA, and 0.05% NP-40 (Wash Buffer). Eluted DNA was reverse cross-linked and treated with 0.2 mg/ml proteinase K (Qiagen) for 2 h at 60°C and heat inactivated at 95°C for 15 min. DNA was extracted with QIAquick PCR purification kit (Qiagen). DNA elution was used in qPCR analysis to measure the abundance of specific DNA sequences.

2.15 Co-culture Experiment

PC3 cells were treated with vehicle, Palbociclib (10 μ M), and Docetaxel (10 nM) for 2 days. Then, cells were washed and re-seeded in 24-well plates at 50,000 seeding density. 2×10^5 BM-MDSC, BMDC, and BMDM were seeded into a 0.4 μ m cell culture insert (Falcon, 353495) and co-cultured with PC3 cells in the bottom chamber. Two days post-co-culturing, BM-MDSC, BMDC, and BMDM cells were collected, and the CD63 mCherry signal was detected by FACS analysis. The human mtDNA was analyzed by quantitative PCR with human mtDNA primers (ND1) and normalized to mouse nuclear DNA (Tert).

2.16 DNA dot blot

DNA samples were denatured at 99°C for 10 min and, chilled on ice for 5 min, and then spotted onto Hybond-N1 nitrocellulose membranes (ThermoFisher) under vacuum using a 96-well Dot Blot hybridization manifold (BioRad, BIO-DOT Apparatus). The membrane was washed twice in $2 \times$ SSC buffer and dried for 1 h at 80°C. After ultraviolet cross-linking, membranes were blocked with 10% non-fat milk and 1% BSA in PBT (PBS 1 0.1% Tween20) for 1h, followed

by 5mC antibody (Abcam, ab10805) (1:1000) incubation overnight at 4°C. Membranes were washed four times with PBST and incubated for 1h with HRP-conjugated anti-rabbit secondary antibody. Following treatment with enhanced chemiluminescence substrate, membranes were scanned on the FusionSolo S imaging system (Vilber). To control for loading, membranes were stained with 0.02% methylene blue solution.

2.17 Extracellular vesicles isolation, purification, and characterization

Cells were cultured and expanded in the appropriate medium to isolate EVs. When the cells were at about 40–50% confluence, they were moved to a medium containing 5% EV-depleted FBS, which was obtained by ultracentrifugation of standard FBS at 134,000 g for 16 h at 4 °C followed by filtration through a 0.1 µm vacuum filtration bottle. EVs were isolated from the conditioned medium using sequential ultracentrifugation, as previously described. Briefly, the conditioned medium was centrifuged at 500g for 5 min, 2,000 g for 10 min, and 4,600 g for 20 min at 4 °C to remove dead cells and debris. The medium was then ultracentrifuged at 134,000 g for 70 min at 4 °C using a Beckman ultracentrifuge and SW32Ti rotor. The pellet was washed in 35 ml PBS and ultracentrifuged again at 134,000 g for 70 min at 4 °C. The resulting EV preparation was dissolved in either PBS or RIPA buffer (Sigma), depending on the application, and either used immediately or stored at –80 °C. The average EV yield obtained from 4T1, PyMT-IK1, MDA-MD-231, E0771-LG, BMDCs, and MEFs was 7.3, 0.8, 0.8, 1.8, 0.1 and 1 µg (determined by BCA) per ml of cell culture medium, respectively.

2.18 Extraction and quantification of plasma cfDNA

cfDNA was extracted from 600 µL of conditioned medium and 100 µL of human/murine plasma using MagMAX Cell-Free DNA Isolation Kit (ThermoFisher Scientific, A29319). In brief, the blood samples are centrifuged at 1600 × g for 10 minutes at 4°C, and the collected plasma samples are centrifuged at 16,000 × g for 10 minutes at 4°C. Proteinase K was added to

100 μ l plasma and incubated at 60°C for 20 minutes. After incubation, Binding Solution/Beads Mix is added. The tubes are placed on the vortex adaptor and shaken for 10 minutes at medium speed to bind the cfDNA to the beads. The beads are washed in 500 μ L of MagMAX™ Cell Free DNA Wash Solution for once and 80% ethanol for two times. In the end, the binding cfDNA is eluted with 50 μ L of MagMAX™ Cell-Free DNA Elution Solution. The concentration of cfDNA was measured using a Qubit dsDNA HS Assay Kit with Qubit 4.0 Fluorometer (ThermoFisher Scientific). The absolute copy numbers were measured using quantitative PCR using indicated primers. The copy number was calculated using the standard curves for cloned Tert and Dloop in a pMD19-T Easy vector (TaKaRa, 3271), respectively. Primer sequences are shown above.

2.19 Gene Expression Profiling

RNA was then extracted using TRIzol RNA isolation reagent (Invitrogen, Cat n=15596026), and RNase-Free DNase set (Qiagen, Cat n=79254) treatment was performed following manufacturers' guidelines. RNA sequencing was performed at the Institute of Oncology Research using the NEBNext Ultra Directional II RNA library preparation kit for Illumina and sequenced on the Illumina NextSeq500 with single-end, 75 base pair long reads. The overall quality of sequencing reads was evaluated using FastQC. STAR (v.2.7.10a)⁸⁹ was used to sequence alignments to the reference mouse genome (GRCm39). Gene Transfer File (GTF) vM27 by Gencode was used to quantify gene expression at the gene level. Further analysis were performed in R Statistical environment (v.4.1.0). Genes without counts were removed for the analysis, and differential expression analysis was performed using DESeq2. In DESeq2 function, the parameter independent Filtering was set up to TRUE to remove genes with low mean normalized counts. Pathway analysis was performed using Camera⁹⁰ and custom gene signature of MDSC functions from different works 22348096, 32086381, 33526920, 27381735, 31533831. All graphical representations were edited using ggplot2 and pheatmap functions.

2.20 Statistical analysis

All values are expressed as the mean and SEM. Statistical analysis was performed with the unpaired t-test for two groups or one-way ANOVA (GraphPad Software) used for multiple groups, with all data points showing a normal distribution. A two-way ANOVA was used for experiments with two independent variables in combination. The researchers were not blinded to the allocation of treatment groups when performing experiments and data assessment. Sample sizes were selected based on preliminary results to ensure adequate power. p values < 0.05 were considered significant.

3. Results

3.1 Senescent cells release mtDNA to cytoplasm and extracellular space

To assess whether mtDNA is released in the cytoplasm of cells undergoing different non-lethal senescent types, we used mouse embryonic fibroblasts (MEFs) where senescence was induced by loss of tumor suppressor gene *Pten* (PICS), overexpression of oncogenic *HRasV12* (OIS), and treatment with the CDK4/6 inhibitor Palbociclib (Palbo), a prototypical TIS that does not induce DNA damage^{91,92}. In all the cases analyzed, senescent cells showed increased SA- β -Gal positivity and p21, and p27 levels but without affecting the Caspase 3 and PARP cleavage and Annexin V staining (Fig. 1A-F).

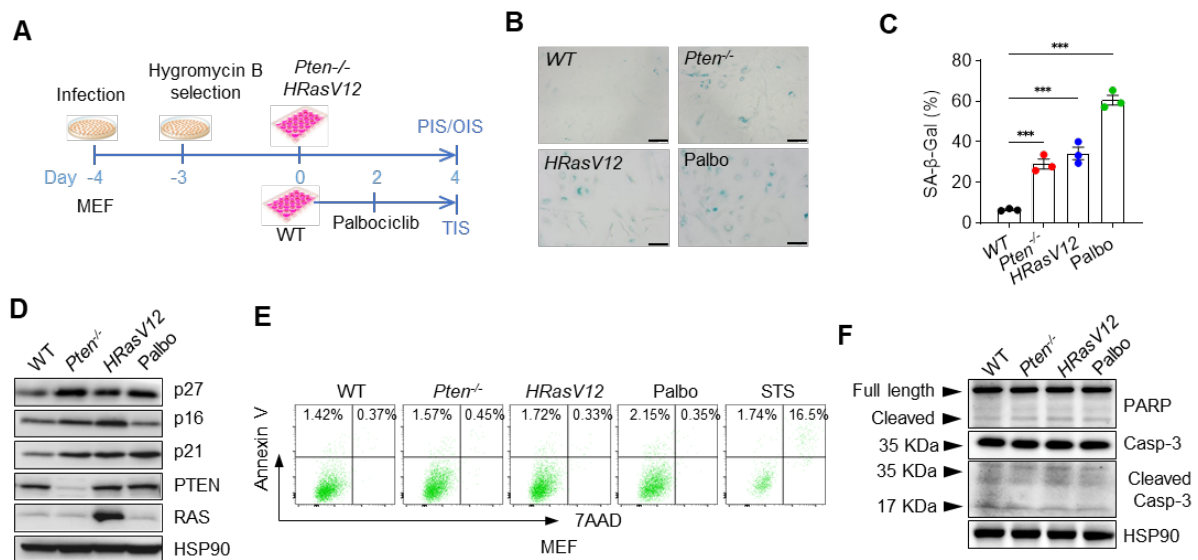


Fig 1. Establishment of senescent models in MEFs.

(A) Scheme of timeline and experimental design of PIS, OIS, and TIS construction in *Pten*^{fl/fl} MEFs. (B and C) Representative images of SA- β -gal of three different senescent types (scale bar: 200 μ m) (B) with quantification in the percentage of SA- β -gal positive cells (C), n = 3 per group. (D) Western blot of indicated senescent markers in senescent MEFs. (E) Representative flow cytometry pattern of Annexin V/7AAD double staining in senescent MEF cells. Cells were treated with 1 μ M of Staurosporine for 12h as a positive control. (F) Western blot of indicated apoptosis markers in senescent MEFs. One-way ANOVA followed by Tukey's multiple comparisons test was used in B. *p < 0.05; **p < 0.01; ***p < 0.001; ns, not significant.

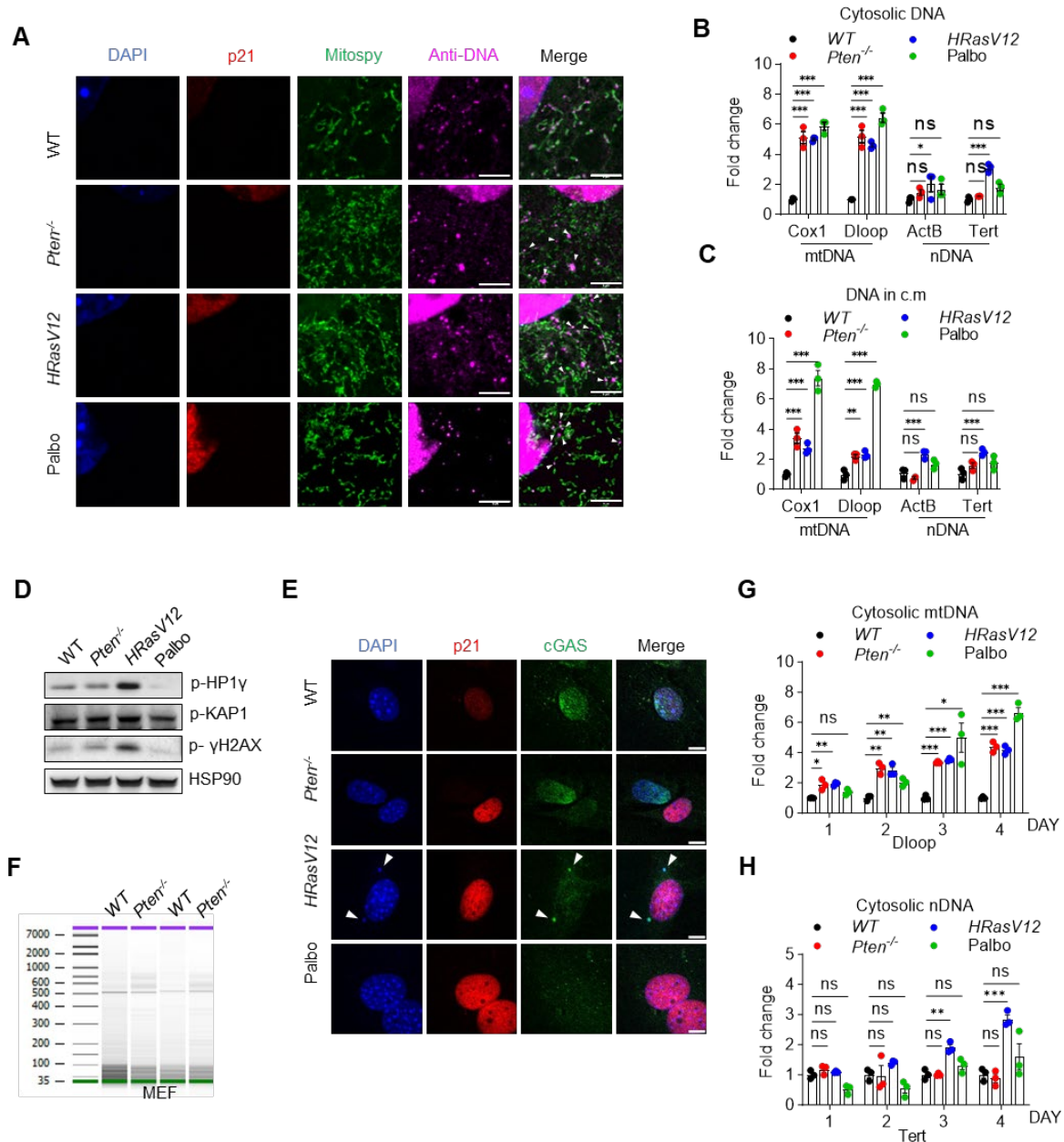


Fig 2. Senescent MEFs release fragmented mtDNA to cytosol and culture media.

(A) Confocal microscopy images of indicated staining in senescent MEFs. White arrows indicate cytosolic DNA. Scale bar: 5 μ m. (B) Quantification of cytosolic mtDNA and nDNA in senescent MEFs. (C) Quantification of mtDNA and nDNA in conditioned medium (c.m) collected from indicated senescent MEFs. (D) Western blot analysis of DNA damage markers in senescent MEFs as indicated. (E) Confocal microscopy images of indicated staining in senescent MEFs. White arrows indicate CCF in OIS. Scale bar: 10 μ m. (F) The size distribution of CM-DNA from WT and *Pten*^{-/-} MEFs was analyzed by Bioanalyzer 2100. (G and H) Quantification of cytosolic Dloop (mtDNA) (G) and Tert (nDNA) (H) change in different time points during senescence induction. One-way ANOVA followed by Tukey's multiple comparisons test was used in B, C, G, H. * $p < 0.05$; ** $p < 0.01$; *** $p < 0.001$; ns, not significant.

Notably, the senescent cells exhibited a marked accumulation of cytosolic DNA (indicated by anti-dsDNA antibody) outside the mitochondria (MitospY) (Fig. 2A). We next checked whether the DNA accumulating in the cytosolic fraction of senescence cells was of nuclear or mitochondrial origin by performing qPCR using mitochondrial (Cox1, Dloop) and nuclear (ActB, Tert) specific primers and immunofluorescence staining for DAPI and cGAS to detect CCFs. Cytosolic mtDNA was increased in all the senescent cells analyzed (Fig. 2B). In contrast, cytosolic nDNA was only increased in OIS (Fig. 2B), in line with previous evidence demonstrating an increased nuclear DNA damage and CCF accumulation in this senescent model^{39,63} (Fig. 2D, E). Of note, we found that in all the different types of senescent cells, mtDNA was more abundant than nDNA (Fig. 2B). In addition, senescent cells also released more mtDNA than nDNA into the extracellular milieu as detected by qPCR in the conditioned media (c.m) from different senescent cells (Fig. 2C). Interestingly, released mtDNA from senescent cells was hyper-fragmented when compared to control as assessed by Bioanalyzer on c.m DNA (Fig. 2F). We next performed a time course experiment and found that mtDNA release occurred at early time points during senescence establishment in all the senescent models (Fig. 2G). Note that in OIS, where both mtDNA and nDNA were increased, mtDNA release even preceded that of nDNA (Fig. 2G, H).

3.2 mtDNA is required for senescence induction and activate cGAS-STING pathway to regulate SASP

To understand whether mtDNA is required for the establishment of cellular senescence, we depleted mtDNA in MEFs undergoing PICS, OIS, and TIS through the overexpression of the Herpes Simplex Virus exonuclease UL12.5 that specifically eliminates mtDNA without affecting nDNA⁹³ (Fig. 3A). Depletion of mtDNA significantly decreased SA- β -Gal positivity (Fig. 3B, C), the p16 and p21 protein levels (Fig. 3D), and the expression of different SASP-associated genes in all the senescence models (Fig. 3E, F).

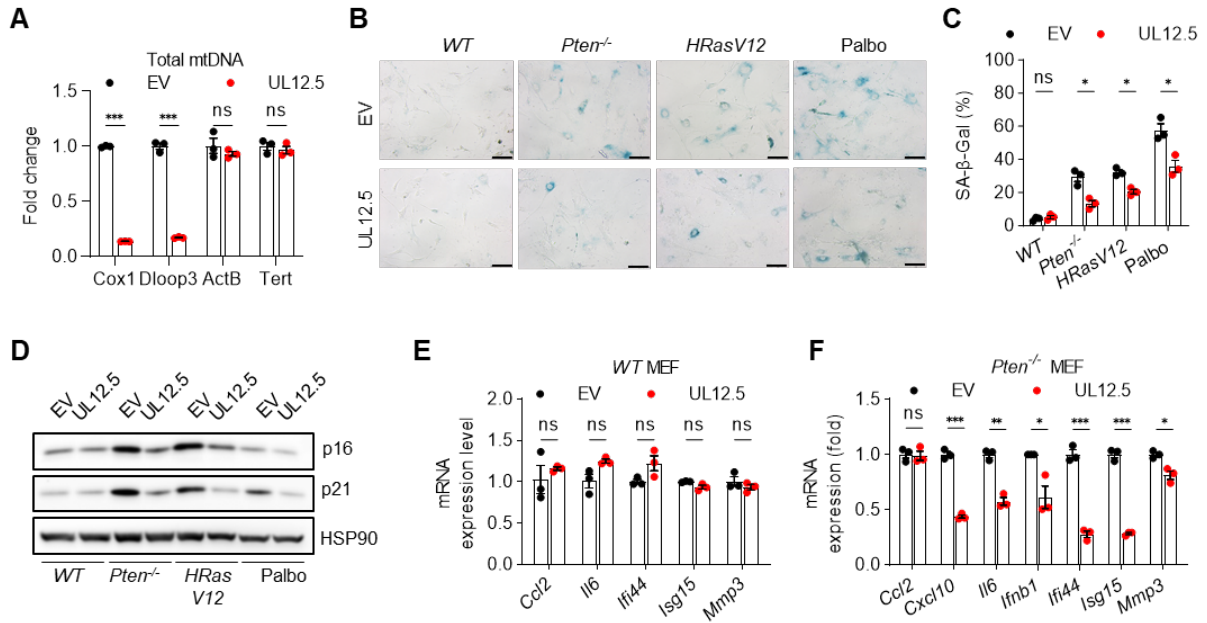


Fig 3. mtDNA is essential for senescence induction.

(A) qPCR analysis of total mtDNA and nDNA in MEF cells after HSV1 UL12.5 or empty vector (EV) lentivirus infection. (B and C) MEFs were transduced with HSV1 UL12.5 or empty vector (EV), and senescence was induced as aforementioned. SA-β-gal staining (B) and quantification (C) were examined in the indicated models. (D-F) MEFs were transduced with HSV1 UL12.5 or empty vector (EV), and senescence was induced as aforementioned. The protein (D) and SASP gene expression (E and F) were examined in the indicated models. Multiple unpaired t-test was used in A, C, E, and F * $p < 0.05$; ** $p < 0.01$; *** $p < 0.001$; ns, not significant.

We next hypothesized that increased mtDNA release in senescent cells could activate the cGAS-STING pathway as previously reported for CCF in OIS^{63,94}. Immunoprecipitation of cGAS in the cytoplasmic fraction of control and senescent cells showed an increased binding of mtDNA rather than nDNA to cGAS in PICS and TIS (Fig. 4A-C). Meanwhile, in OIS, we detected both mtDNA and nDNA bound to cGAS, in line with previous evidence⁶³ (Fig. 4B, C). Knockdown of cGAS (via short-hairpin *shMb21D1*) in MEFs infected with Cre, HRasV12, or treated with Palbo reduced the expression of SASP genes in all the models analyzed (Fig. 4D-F). Together, these findings demonstrate that cytosolic mtDNA release is required for senescence induction and activation of the SASP.

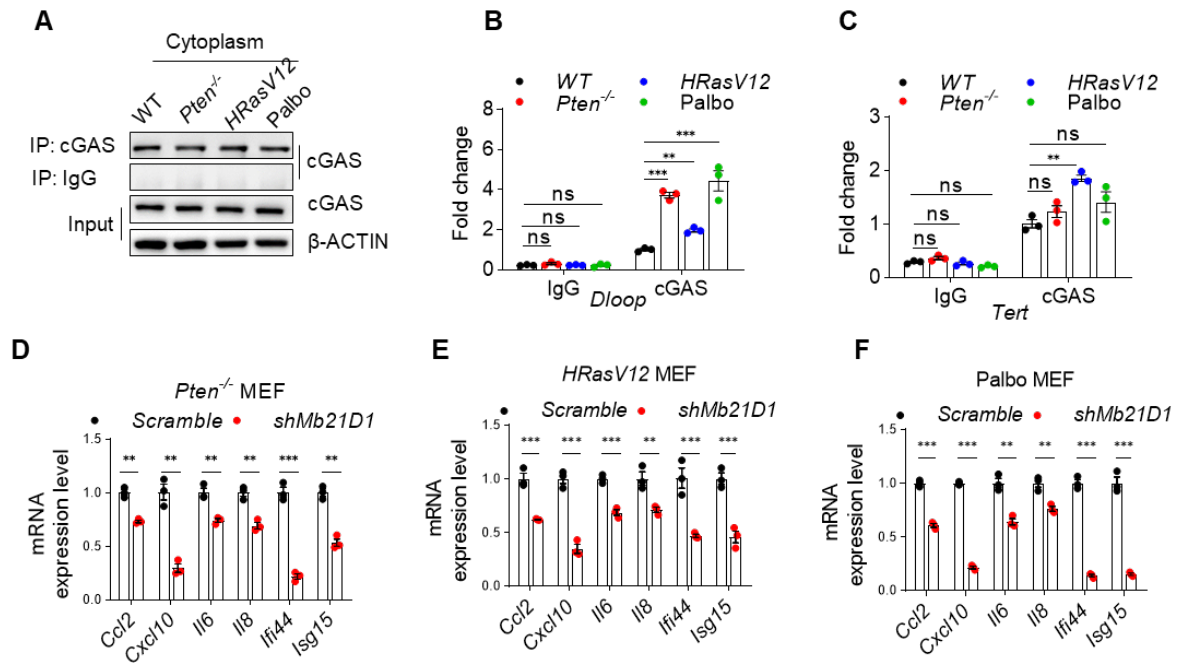


Fig 4. Cytosolic mtDNA activates the cGAS-STING pathway to regulate SASP.

(A) Cytoplasm of senescent MEFs were immunoprecipitated with anti-cGAS antibody or rabbit IgG. Immunoblot analysis of cGAS precipitation was shown. (B and C) Precipitated DNA was amplified by real-time qPCR using the indicated primer pairs. (D-F). MEFs were transduced with cGAS shRNA or scramble vectors, and senescence was induced as aforementioned. SASP gene expression was examined in the indicated models. All values are presented as the mean \pm SEM. Multiple unpaired t-tests were used in D-F. Two-way ANOVA followed by Dunnett's multiple comparisons test was used to evaluate the statistical significance in B and C. * $p < 0.05$; ** $p < 0.01$; *** $p < 0.001$; ns, not significant.

3.3 Senescent tumor cells release mtDNA to cytosol and extracellular space

As senescence is commonly observed in cancer chemotherapy, we were wondering whether mtDNA can also be released in senescent tumor cells. We further validated the previous data in both murine and human prostate tumor cells (TRAMP-C1 and PC3) treated with Palbociclib or Docetaxel in low dosage to induce cellular senescence but not apoptosis (Fig 5A-E). Consistent with the observation in senescent MEFs, Palbociclib treatment also induced cytosolic mtDNA release in senescent tumor cells, as well as in the culture media. Meanwhile, docetaxel treatment increased the release of both mtDNA and nDNA (Fig 5F-I). However, docetaxel-treated TRAMP-C1 cells released a higher amount of mtDNA than nDNA in the cytosol and the culture media ((Fig 5F-I).

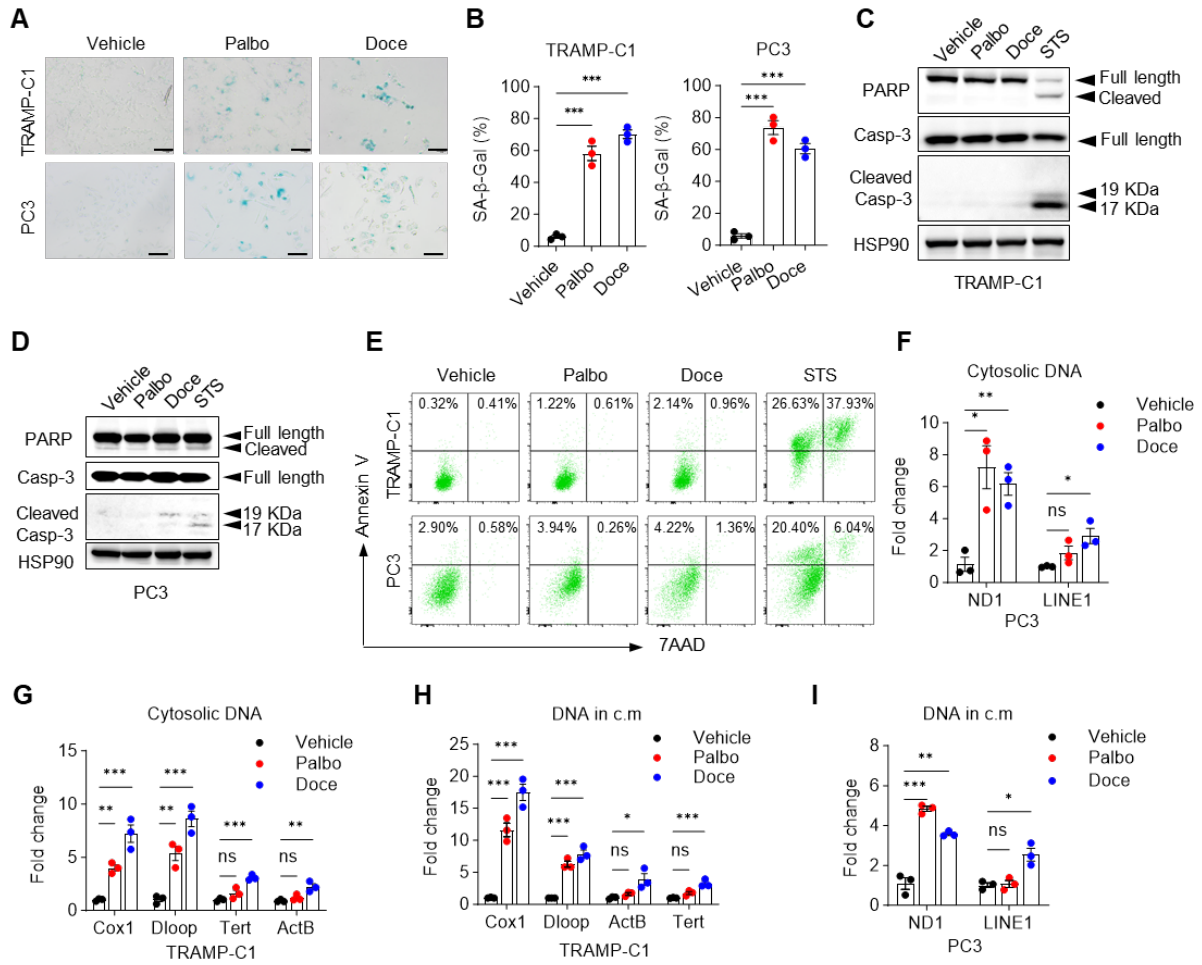


Fig 5. Senescent tumor cells also release mtDNA to cytosol and culture media.

(A) Representative images of SA-β-gal staining in TRAMP-C1 and PC3 cells treated with 2.5 μM Palbociclib (Palbo) or 10 nM Docetaxel (Doce) for 48 h. Scale bar: 100 μm. (B) Quantification of SA-β-gal staining in TRAMP-C1 cell treated with 2.5 μM Palbociclib (Palbo) or 10 nM Docetaxel (Doce) for 48 h. Scale bar: 100 μm. (C and D) Western blot of indicated markers in TRAMP-C1 and PC3 cells aforementioned. (E) Representative flow cytometry pattern of Annexin V/7AAD double staining in senescent prostate tumor cells. Cells were treated with 1 μM of Staurosporine for 12h as a positive control. (F and G) Quantification of cytosolic mtDNA and nDNA in TRAMP-C1 (F) and PC3 (G) cells treated with Palbo and Doce. (H and I) Quantification of mtDNA and nDNA in c.m. collected from TRAMP-C1 (H) and PC3 (I) cells treated with Palbo and Doce, as mentioned before. Data pooled from one experiment representative of at least three independent experiments (A, C-I) or three independent experiments (B) are shown (mean ± SEM). One-way ANOVA followed by Tukey's multiple comparisons test was used in B, F-I. *p < 0.05; **p < 0.01; ***p < 0.001; ns, not significant.

Moreover, consistent with the data in senescent MEFs, depletion of mtDNA in TRAMP-C1 cells infected with UL12.5 and treated with Palbociclib abrogated senescence induction and SASP

genes expression (Fig. 6A-D). Together, these data highlight the crucial role of mtDNA in senescence in both primary MEFs and cancer cells.

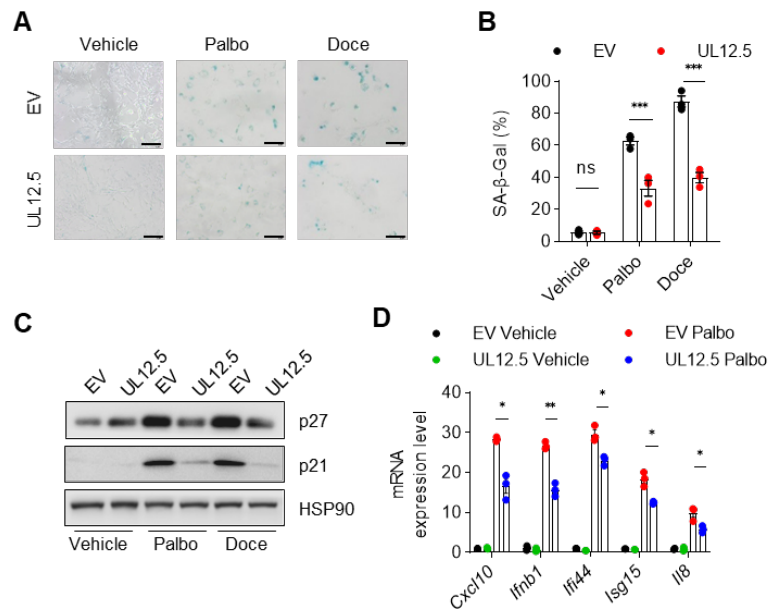


Fig 6. mtDNA is essential for senescence induction in tumor cells.

(A and B) TRAMP-C1 cells were infected with HSV1 UL12.5 or empty vector (EV) lentivirus. SA-β-gal staining (A) and quantification (B) were examined in TRAMP-C1 EV and TRAMP-C1 UL12.5 cells treated with Palbo or Doce. (C and D) The indicated protein (C) and SASP gene expression (D) were examined in the aforementioned cells. All values are presented as the mean ± SEM. Multiple unpaired t-test was used in B. Two-way ANOVA followed by Dunnett's multiple comparisons test was used to evaluate the statistical significance in D. *p < 0.05; **p < 0.01; ***p < 0.001.

3.4 Senescent tumor cells released mtDNA is uptaken by PMN-MDSCs

Senescent cells have been shown to exert detrimental effects on the tissue microenvironment, contributing to tumorigenesis through different mechanisms^{21,29}. In prostate cancer, we and others have shown that senescent tumor cells enhance the recruitment of diverse populations of myeloid cells^{1,33,95}. As demonstrated, PMN-MDSCs are the main myeloid immune subset infiltrating both mouse and human prostate cancers, whereas T and NK cells are scarce^{1,33}. To better characterize the role of mtDNA released by senescent tumor cells in the tumor microenvironment, we assessed whether extracellular mtDNA could be uptaken by myeloid cells through a trans-species experiment using human prostate tumor cells injected in NRG

mice. We injected PC3 cells in NRG mice and treated them with or without Palbociclib to induce senescence *in vivo* (Fig. 7A). Different populations of murine myeloid cells were then sorted from tumors of untreated and treated mice by using the following markers: CD11b⁺CD11c⁺ (dendritic cells), CD11b⁺F4/80⁺ (macrophages), and CD11b⁺ Ly6G⁺ (PMN-MDSCs) (Fig. 7B). Finally, qPCR analysis was performed in the different immune subsets to detect mtDNA using human-specific primers. We found that in mice treated with TIS, tumor-infiltrating CD11b⁺ Ly6G⁺ cells accumulate a significantly higher amount of human mtDNA (ND1) compared to other sorted immune populations (Fig. 7C, D). Of note, no change of human nuclear DNA (LINE1) was detected in the sorted immune cell populations, thereby validating our previous findings in the c.m of cells treated with Palbo (Fig. 5H, I).

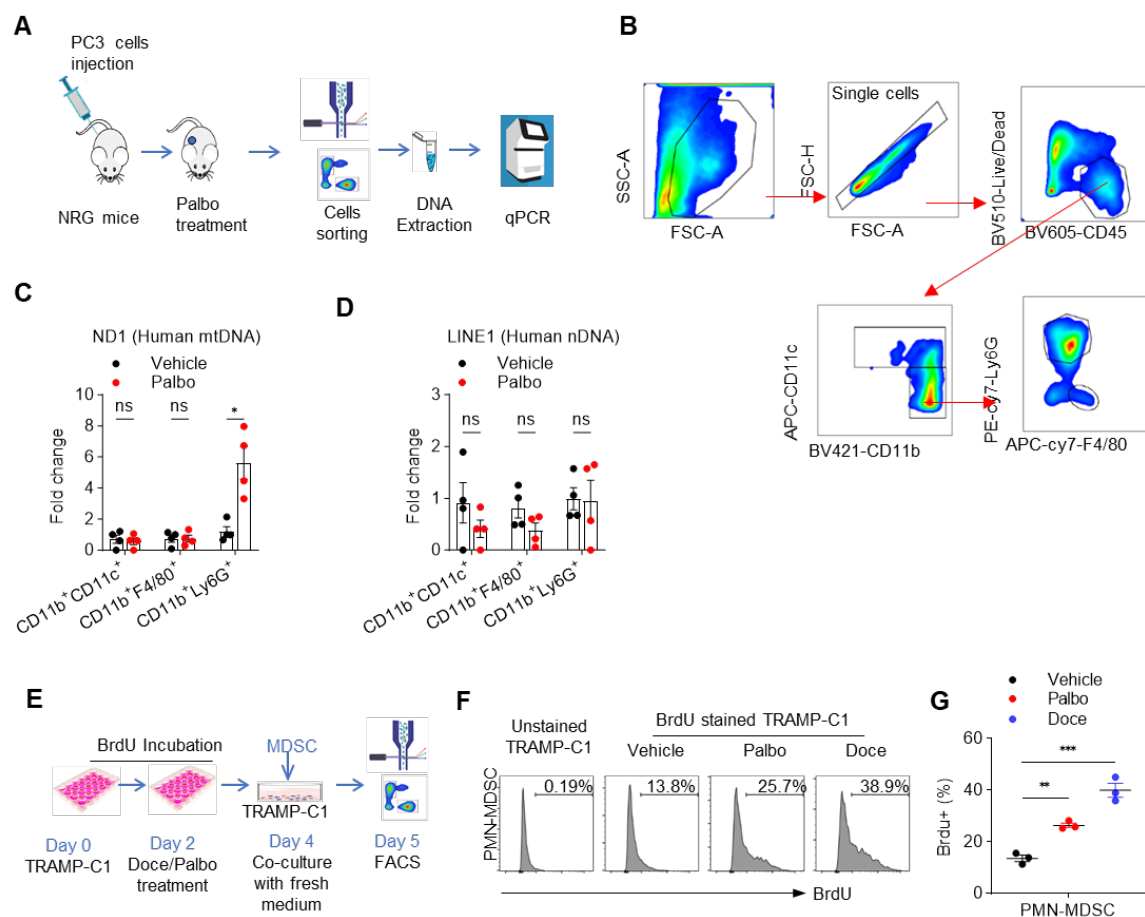


Fig 7. Senescent cells released mtDNA, which is uptaken by PMN-MDSC.

(A) Scheme of experimental design. (B) Gating strategy for mouse CD11b⁺CD11c⁺; CD11b⁺F4/80⁺ and CD11b⁺Ly6G⁺ myeloid cells from tumor xenograft in NRG mice. (C and D) Fold changes of human mtDNA (ND1)

and nDNA (LINE1) were quantitated by q-PCR using specific primers and normalized to mouse total DNA in CD11b⁺ CD11c⁺, CD11b⁺ F4/80⁺ and CD11b⁺ Ly6G⁺ myeloid cells which were obtained from PC3 tumor. (E) Scheme of timeline and experimental design. (F and G) Representative flow cytometry pattern and quantification of BrdU signal in BM-MDSC co-cultured with senescent TRAMP-C1 cell. Multiple unpaired t-tests were used in C and D. One-way ANOVA followed by Tukey's multiple comparisons test was used in G. *p < 0.05; **p < 0.01; ***p < 0.001.

These data were validated using murine TRAMP-C1 and BM-MDSCs cells *in vitro*. To perform this experiment, murine TRAMP-C1 was pre-incubated with BrdU to label the DNA before treatment with Palbo and Doce (Fig. 7E). After the senescence was induced by Palbociclib and Docetaxel treatment, BM-MDSC were co-cultured with the BrdU labeled TRAMP-C1 cells in the fresh culture media (Fig. 7E). We then detected the BrdU in MDSCs by FACS analysis, and the BM-MDSCs co-cultured with senescent TRAMP-C1 cell showed an increased BrdU signal, which indicated the presence of tumor cells derived DNA (Fig. 7F, G). Together, these data suggest that senescent cells released extracellular mtDNA can be uptaken by PMN-MDSCs.

3.5 Senescent tumor cells released mtDNA is packaged in extracellular vesicles (EVs)

Senescent cells are reported with increased extracellular vesicles (EVs) production in multiple models of cellular senescence^{96,97}. To explore the mechanism that mtDNA release outside the cells and uptaken by PMN-MDSC, we isolated the EVs in the c.m collected from senescent cancer cells and MEFs by ultracentrifuge. In line with previous research, we observed increased EVs amount in c.m from senescent cells compared to that from proliferating cells (Fig. 8A, C). In addition, qPCR performed with an equal number of EVs from senescent and non-senescent cells showed increased mtDNA content in each senescence-associated EV. In contrast, nDNA was increased only in the cells treated with Docetaxel (Fig. 8B, D).

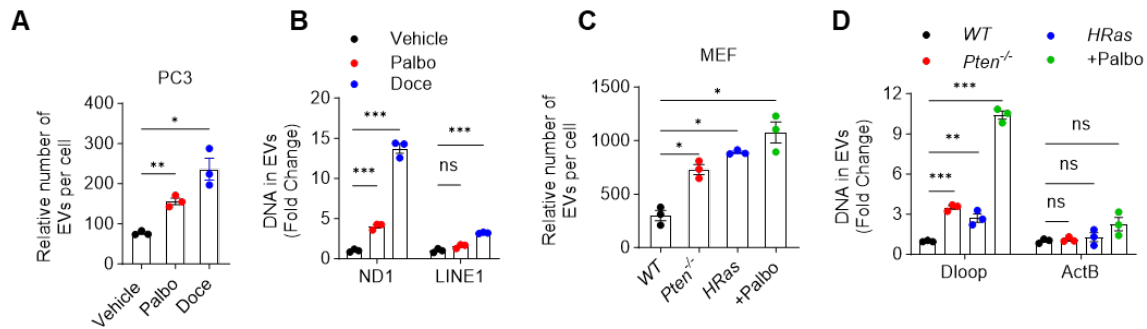


Fig 8. Senescent cells release mtDNA, which is packed in EVs.

(A) EVs amount in the c.m from TRAMP-C1 cells treated with Palbo or Doce is normalized to the total cell number. (B) Fold change of human mtDNA (ND1) and nDNA (LINE1) in the same amount of EVs from the senescent cell aforementioned. (C) EVs amount in the c.m from senescent MEFs is normalized to the total cell number. (D) Fold change of mtDNA (Dloop) and nDNA (ActB) in the same amount of EVs from the senescent cell aforementioned. One-way ANOVA followed by Tukey's multiple comparisons test was used in A-D. * $p < 0.05$; ** $p < 0.01$; *** $p < 0.001$.

To further validate these findings *in vitro*, we then constructed a PC3 cell line expressing CD63-mCherry that labels extracellular vesicles. The PC3 CD63-mCherry cells were pre-treated with Palbo and Doce to induce cellular senescence and following co-cultured with bone marrow-derived murine MDSCs (BM-MDSCs), DCs (BMDCs) and macrophages (BMDMs) in transwells, respectively (Fig. 9A, B). Both BM-MDSCs and BMDM increased the EVs uptaken when the cancer cells were treated with Palbo and Doce (Fig. 9C). While BMDCs did not show as high EVs uptake as BM-MDSCs and BMDM. Consistent with *in vivo* data, qPCR analysis showed an increased accumulation of human mtDNA only in BM-MDSCs but not in BMDMs (Fig. 9D). This might be due to the higher acidification of phagosomal lumen and faster DNA degradation in macrophage^{98,99}.

Next, we treated the senescent PC3 CD63-mCherry cells with GW4869 to inhibit EVs release¹⁰⁰ and then co-cultured with BM-MDSC. Blockage EVs release by GW4869 reduced the mCherry signal and human mtDNA accumulation in BM-MDSC after co-cultured with senescent PC3 cells (Fig. 9E, F). Then, we further validated whether PMN-MDSC can also capture senescent tumor cells released EVs *in vivo*. By injecting the PC3 CD63-mCherry cells in NRG mice

followed by Palbociclib treatment, we also detected the EVs uptake capacity of different myeloid cells in TME. Interestingly, by measuring the mCherry signal through flow cytometry, CD11b⁺F4/80⁺ (macrophages) and CD11b⁺ Ly6G⁺ (PMN-MDSCs) showed significantly higher EVs capture capacity compared to CD11b⁺CD11c⁺ (dendritic cells). However, only PMN-MDSCs showed an increased mCherry signal in the mice treated with Palbociclib (Fig. 9G), which is consistent with our previous data that increased mtDNA uptake only observed in PMN-MDSC (Fig. 7C). Collectively, these results suggest that PMN-MDSCs are capable of internalizing extracellular mtDNA that originates from both human and murine senescent tumor cells.

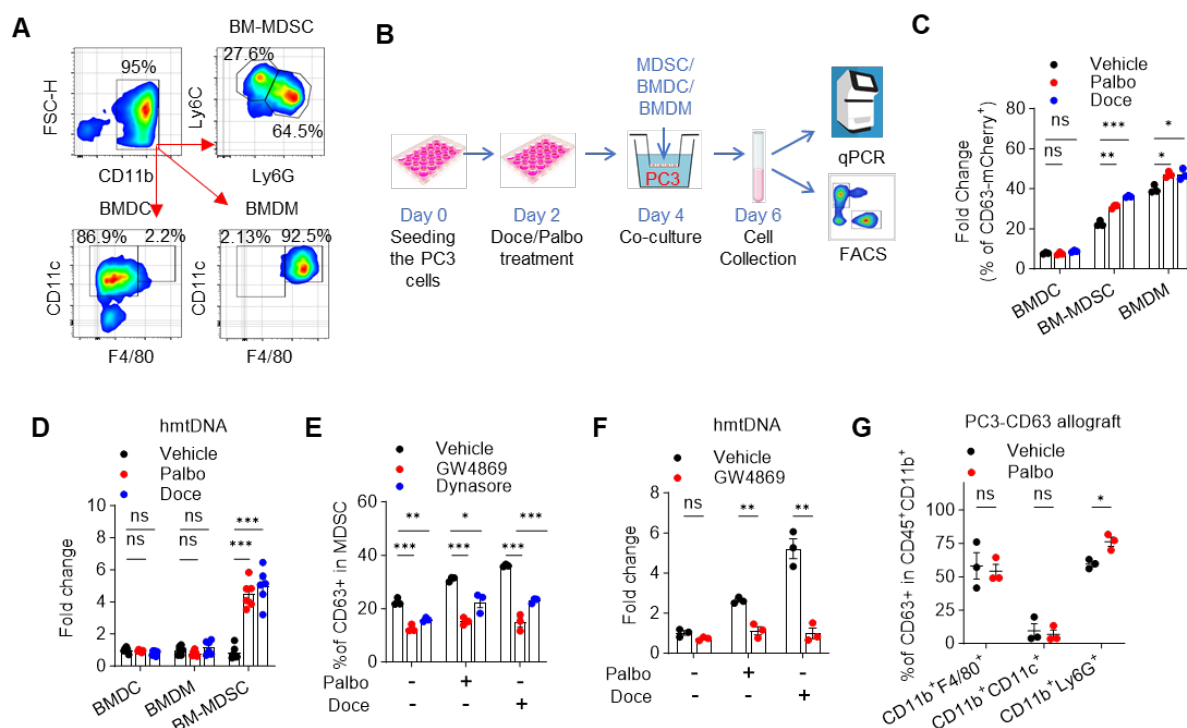


Fig 9. PMN-MDSCs uptake senescent cells derived mtDNA through EVs

(A) Representative flow cytometry pattern of BM-MDSC, BMDC, and BMDM differentiation quality *in vitro*. (B) Scheme of timeline and experimental design of human PC3 cell co-cultured with mouse BM-MDSC, BMDC, and BMDM. (C and D) The ratio of CD63-mCherry positive cells (C) and human mtDNA (D) in BMDC, BM-MDSC, and BMDM co-cultured with PC3-CD63-mCherry cells pretreated with Palbo or Doce. (E) The ratio of CD63-mCherry positive cells in BM-MDSC co-cultured with PC3-CD63-mCherry cells pretreated with Palbo or Doce in the presence of 10uM GW4869. (F) qPCR analysis of human mtDNA in BM-MDSC co-cultured with PC3-CD63-mCherry cells pretreated with Palbo or Doce in the presence of 10uM GW4869. (G) The ratio of CD63-mCherry positive cells was quantitated in CD11b⁺ CD11c⁺, CD11b⁺ F4/80⁺, and CD11b⁺ Ly6G⁺ myeloid cells,

which originated from the PC3 tumor. One-way ANOVA followed by Tukey's multiple comparisons test was used in C-E. Multiple unpaired t-test was used in F and G * $p < 0.05$; ** $p < 0.01$; *** $p < 0.001$.

3.6 MtDNA released by senescent tumor cells enhances the immune suppressive function of MDSCs

Having demonstrated that the MDSCs internalize mtDNA derived from senescent tumor cells, we investigated whether senescent cells could affect MDSCs function through the extracellular release of mtDNA. To address this, we isolated the EVs from c.m collected from senescent tumor cells to treat BM-MDSCs and perform an immunosuppressive assay using splenic T cells. BM-MDSCs treated with EVs from senescent cells showed an increased immunosuppressive capability in comparison to c.m from non-senescent cells (Pablo vs. Veh) (Fig. 10A). To distinguish the effect of mtDNA and SASP factors contained in EVs, we directly delivered mtDNA extracted from c.m of senescent cells in BM-MDSCs through lipid-based transfection. Transfection of mtDNA significantly in BM-MDSCs enhanced their T cell immunosuppressive ability and increased the expression of immunosuppressive-related genes (*Arg1*, *iNos2*, *Cd274* (Encodes PD-L1)), pro-inflammatory genes (*Il6*, *Il23*) and type I interferon genes (*Ifnb1*, *Cxcl10*) (Fig. 10B, C). This demonstrates that mtDNA can directly promote MDSCs activation, which is independent of the SASP. To better understand the downstream of mtDNA in MDSCs, we isolated the total mRNA from mtDNA treated and untreated BM-MDSCs and performed RNA-Seq. RNA-seq analysis of BM-MDSCs transfected with mtDNA provided evidence that mtDNA exhibited distinct abilities to upregulate pro-inflammatory genes, which were strongly associated with immunosuppressive signatures of MDSCs (Fig. 10D-F). Stimulation of MDSCs with mtDNA also significantly changed the expression levels of several genes involved in immune suppression and tumor promotion, such as IL6/STAT3 and NF- κ B signaling^{101,102} (Fig. 10G).

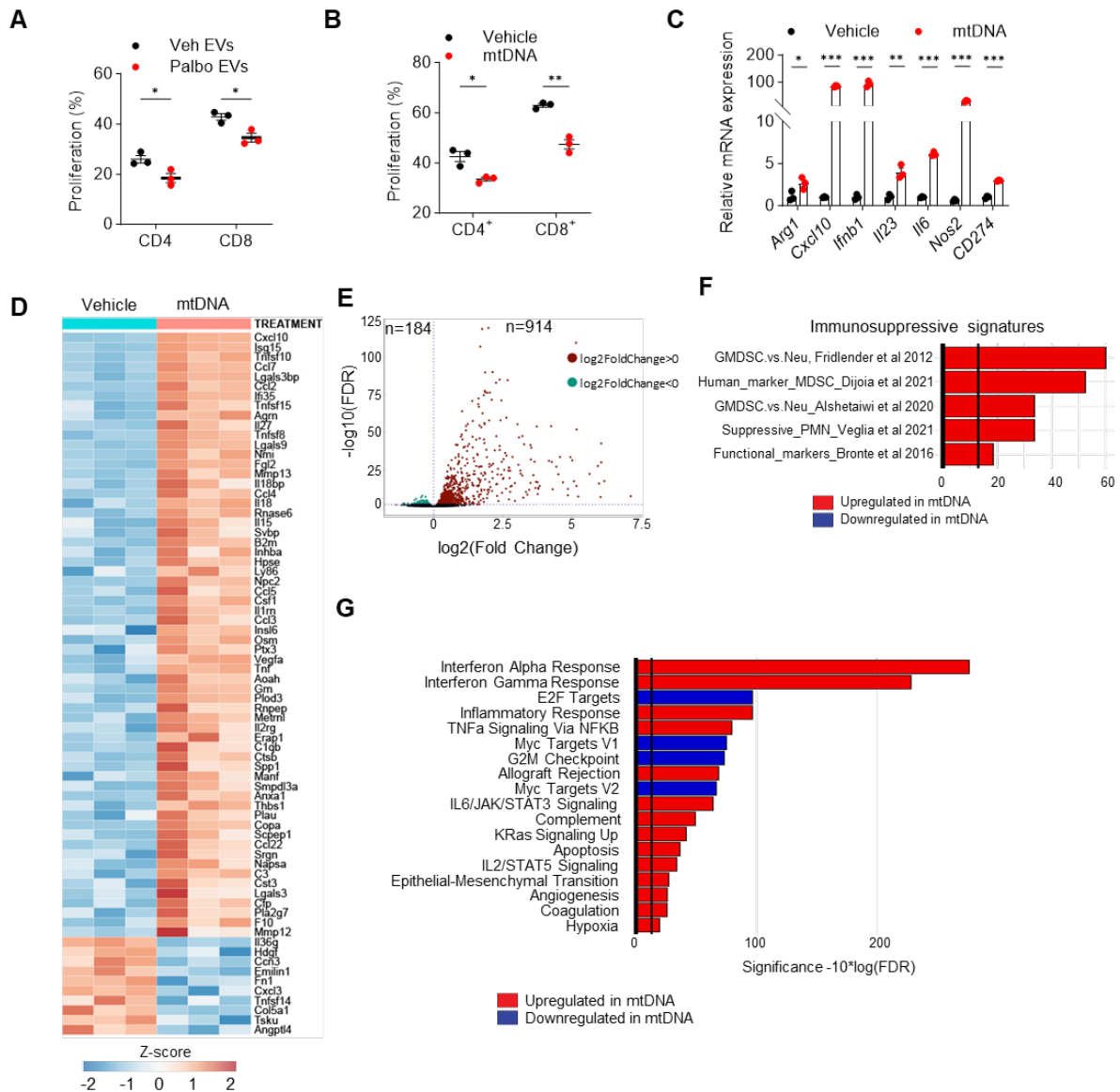


Fig 10. Senescent cells derived mtDNA enhances the immune suppressive function of MDSCs

(A) T cell Suppression assay by BM-MDSC pre-treated with EVs isolated from Palbo treated and untreated TRAMP-C1 c.m. BM-MDSC and splenocytes were seeded at a ratio of 1:10. (B) Quantification of T cell proliferation assay by BM-MDSC pre-transfected with mtDNA at a concentration of 250 ng/ml for 12 h. (C), RT-qPCR analysis of mRNA indicated gene expression levels of BM-MDSC that were transfected with mtDNA, as mentioned before. (D), Heat map of RNA-seq of BM-MDSC transfected with or without mtDNA. The color key represents the normalized Z score. (E) Volcano plot of RNA-seq of BM-MDSC transfected with or without mtDNA. The dots indicate the differentially expressed genes with $\text{Log}_2\text{FoldChange} > 0$ and $\text{FDR} < 0.05$. (F) Immunosuppressive signatures analysis of upregulated genes in previous samples. (G) Pathways/functions changed in BM-MDSC transfected with mtDNA vs. vehicle. Only pathways that were different between groups with $p < 0.01$ adjusted for multiple comparisons are shown. Multiple unpaired t-tests were used in A-C. One-way ANOVA followed by Tukey's multiple comparisons test was used in C-E. Multiple unpaired t-test was used in F and G * $p < 0.05$; ** $p < 0.01$; *** $p < 0.001$. In F, $\text{FDR} < 0.05$.

3.7 MtDNA enhances the immune suppressive function of MDSCs by activating the cGAS-STING-NF- κ B pathway

Intrigued by the increased MDSCs activation of the DNA sensing pathway, we next explored the mechanism by which mtDNA enhances the immune suppressive activity of MDSCs focusing on cGAS and TLR9 (Toll-like receptor 9), two main DNA sensors that can recognize the host cell DNA as a potent damage/danger-associated molecular pattern (DAMP). By transfecting mtDNA in wild-type or TLR9-deficient (*Tlr9*^{-/-}) or cGAS-deficient (*Mb21d1*^{-/-}) BM-MDSCs, we found that mtDNA failed to enhance the levels of immunosuppressive genes in cGAS knock-out MDSCs (Fig. 11A). In contrast, deficiency of TLR9 receptor in BM-MDSCs did not result in an inhibition of MDSCs activation (Fig. 11A). cGAS is a cytosolic DNA sensor that activates innate immune responses by producing the second messenger 2'3'-cGAMP, which activates the adaptor STING and triggers type I interferon response. Indeed, we found mtDNA transfected in BM-MDSC significantly activated the phosphorylation of STING and IRF3 (Fig. 11B). Notably, we also observed the increased phosphorylated STAT1 and STAT3, as well as phosphorylated p65 and IKBa, which indicated the activation of NF- κ B signaling pathway (Fig. 11B). Consistent with previous data, the mtDNA lost the effect on activating these pathways in cGAS deficiency MDSCs (Fig. 11C). In parallel, mtDNA treatment also failed to enhance the immunosuppression ability in cGAS knock-out BM-MDSCs (Fig. 11D).

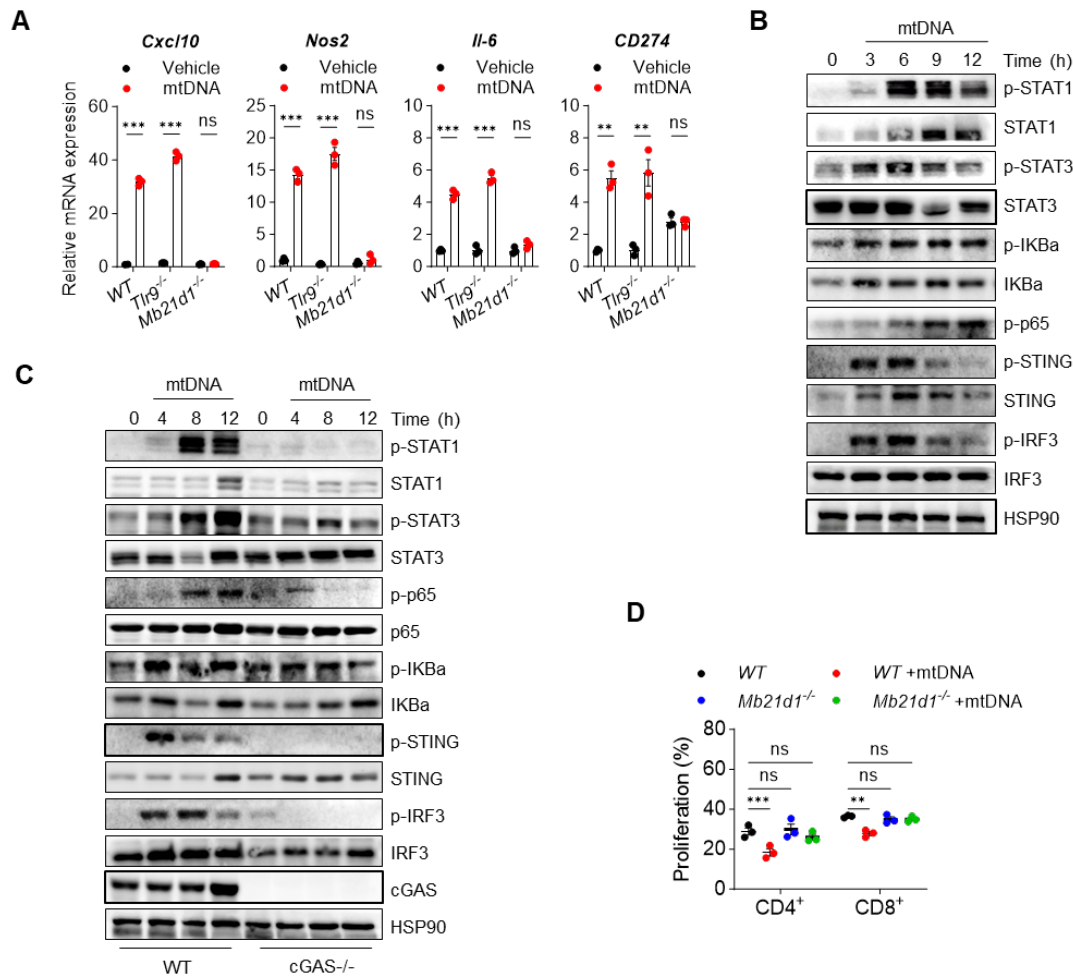


Fig 11. Senescent cells derived mtDNA activates the cGAS-STING pathway in MDSCs

(A) RT-qPCR analysis of the indicated gene expression level in *WT*, *Tlr9*^{-/-} and *Mb21d1*^{-/-} BM-MDSC after mtDNA transfection. (B) WB analysis of cGAS-STING signaling pathway activation in BM-MDSC transfected with mtDNA. (C) WB analysis of cGAS-STING signaling pathway activation in WT and *Mb21d1*^{-/-} BM-MDSC transfected with mtDNA. (D) Quantification of T cell proliferation assay in WT and *Mb21d1*^{-/-} BM-MDSC transfected with mtDNA. Multiple unpaired t-tests were used in A. Two-way ANOVA followed by Dunnett's multiple comparisons test was used to evaluate the statistical significance in D. **p* < 0.05; ***p* < 0.01; ****p* < 0.001.

Activating the cGAS-STING signaling pathway augmented antitumor immunity. The immunosuppressive activity of MDSCs in cancer also has been reported to require inactivation of the type I interferon pathway¹⁰³. We speculated that the enhanced immunosuppressive function of BM-MDSCs upon mtDNA treatment is mainly due to the STING-NF-κB activation. We then assessed the effect of mtDNA on BM-MDSCs after the blockage of NF-κB signaling by using

an NF- κ B inhibitor. Notably, we found that NF- κ B inhibitor pre-treatment in BM-MDSCs resulted in the abrogation of phosphorylated p65, IKBa, STAT1, and STAT3. In contrast, the phosphorylation of STING and IRF3 were retained (Fig. 12A). In parallel, the NF- κ B inhibitor pre-treatment also abolished the enhanced T cell suppressive ability and upregulated immunosuppressive genes expression by mtDNA transfection (Fig 12B, C). Whereas BM-MDSCs were still producing IFN β , which may enhance T cell response. Interestingly, we found that upon mtDNA treatment, BM-MDSCs showed the weakest ability of IFN β mRNA upregulation and production compared with BMDC and BMDM treated with mtDNA (Fig. 12D, E). These results indicate that enhanced immunosuppression in BM-MDSCs upon mtDNA treatment mainly relies on the activation of the cGAS-STING-NF- κ B pathway.

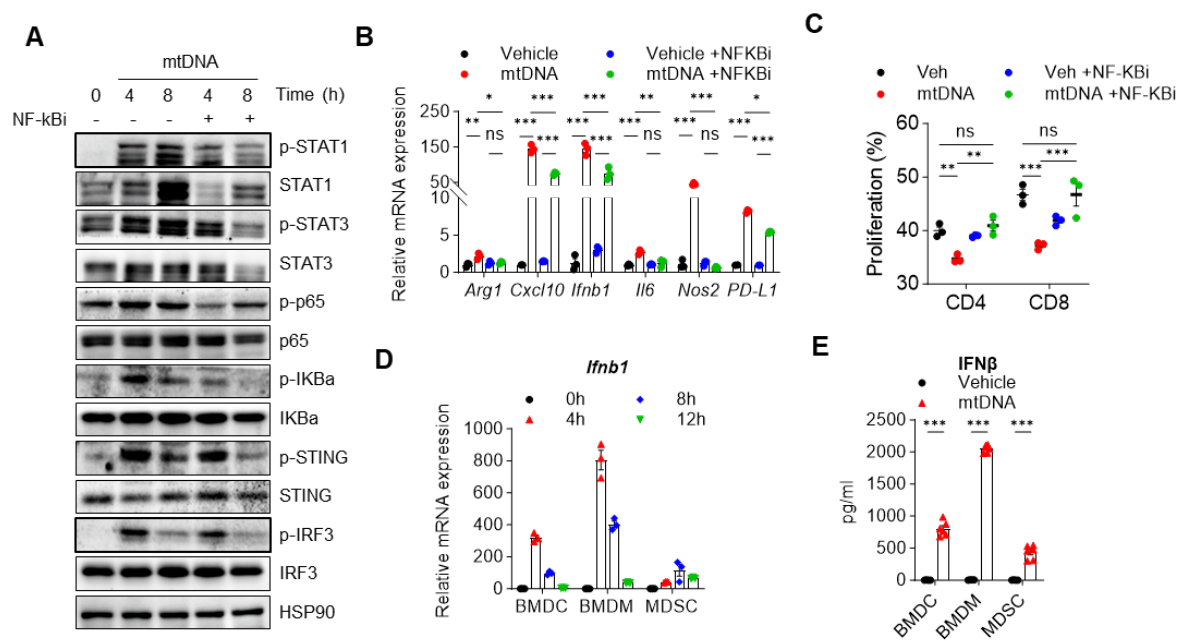


Fig 12. MtdNA enhances the immune suppressive function of MDSCs by activating the STING-NF- κ B pathway

(A) WB analysis of the signaling pathway activation in BM-MDSC transfected with mtDNA in the presence of 10 μ M NF- κ B Activation Inhibitor IV. (B) RT-qPCR analysis of the indicated gene expression in BM-MDSC transfected with mtDNA and with or without NF- κ B Activation Inhibitor IV. (C) Quantification of T cell proliferation assay by BM-MDSC pre-transfected with mtDNA and with or without NF- κ B inhibitor for 12 h. BM-MDSC and splenocytes were seeded at a ratio of 1:20. (D) RT-qPCR analysis of the *Ifnb1* genes' expression at different time points in BM-MDSC, BMDC, and BMDM transfected with mtDNA. (E) ELISA assay of IFN β in

the culture media from BM-MDSC, BMDC, and BMDM transfected with mtDNA. Two-way ANOVA followed by Dunnett's multiple comparisons test was used to evaluate the statistical significance in B and C. Multiple unpaired t-tests were used in E. * $p < 0.05$; ** $p < 0.01$; *** $p < 0.001$.

3.8 mtROS and EndoG regulate mtDNA release in senescent cells

Aiming at identifying potential pharmacological treatments to block the release of mtDNA in the extracellular space, we focused on the mechanism by which mtDNA is produced and released outside the mitochondria. It has been reported that ROS accumulation is associated with mitochondrial dysfunctions during cellular senescence³⁸⁻⁴². We speculate that increased ROS production in mitochondria may cause the release of mtDNA, ultimately leading to mitochondrial dysfunction and chronic inflammation and disease. We first stained CM-H2DCFDA, a fluorescent indicator for ROS, to detect ROS production in the senescent MEFs. FACS analysis showed that ROS production was increased in all the senescence models analyzed (Fig. 13A). It coincides with the increased cytosolic mtDNA that was overserved in all the models. Then, we treated the cell with mito-TEMPO, a mitochondria-targeted antioxidant, to deplete the mtROS during senescence induction. In contrast, the depletion of mtROS by mito-TEMPO prevented cytosolic mtDNA accumulation in PICS and OIS (Fig. 13B-C). In parallel, mito-TEMPO treatment significantly attenuated the senescence, as well as the levels of senescence markers and SASP-associated genes (Fig. 13D-H). To better understand the role of mtROS in mtDNA release and exclude the other influences of impaired mitochondrial function in senescent cells, we directly treated *WT* MEFs with H₂O₂ and detected the cytosolic mtDNA release. Oxidative stress induced by low dosage H₂O₂ (40 μ M for 4 hours following 16-hour recovery) was sufficient to induce cellular senescence and cause the cytosolic mtDNA release in *WT* MEFs (Fig. 13I, J).

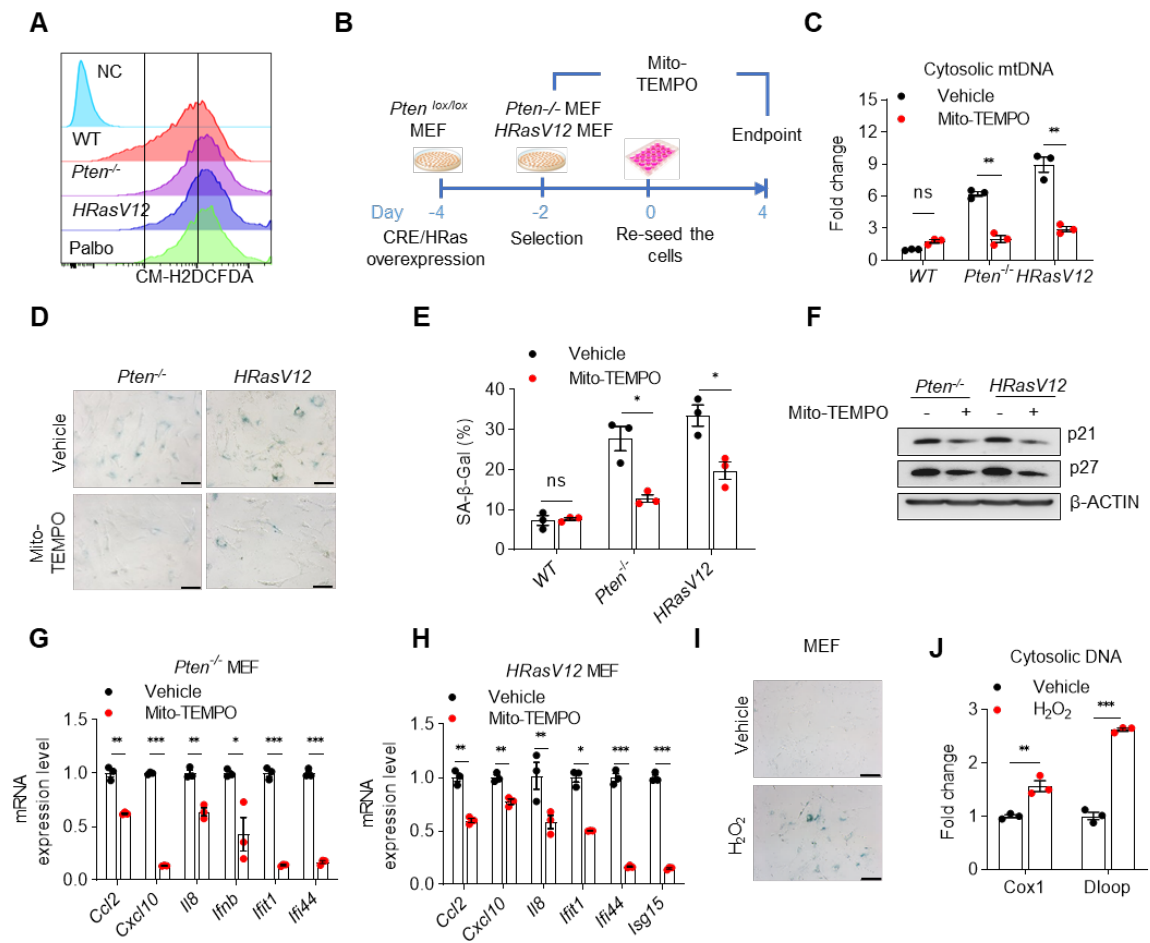


Fig 13. mtROS induces mtDNA release in senescent cells

(A) Fluorescence intensity of senescent MEFs analyzed by flow cytometry after staining with CM-H2DCFDA. (B) Timeline for Mito-TEMPO treatment in *Pten*^{-/-} and HRasV12 MEFs. (C) Quantification of cytosolic mtDNA in senescent MEFs treated with 5 μ M Mito-TEMPO. (D-H) SA- β -gal staining (D) and quantification (E) indicated protein (F) and SASP gene expression (G and H) were detected in senescent MEFs treated with Mito-TEMPO. (I) Representative images of SA- β -gal staining in WT MEFs treated with 40 μ M H₂O₂ for 4 h and 16 h recovery. (J) Quantification of cytosolic mtDNA in MEFs treated with H₂O₂ as aforementioned. All values are presented as the mean \pm SEM. Multiple unpaired t-test was used in C, E, G, H, and J. **p* < 0.05; ***p* < 0.01; ****p* < 0.001; ns, not significant.

In physiological conditions, the cellular pool of mtDNA is maintained by mitochondrial endonuclease G, whose mitochondrial to nuclear re-localization is regulated by ROS^{104,105}. Along with the increased mtDNA release, EndoG also translocated to the nucleus in response to the H₂O₂ treatment in MEFs (Fig. 14A). EndoG is the most abundant and active mitochondrial endonuclease, located in the intermembrane space of mitochondria, and it is

(A) Confocal microscopy images of EndoG nuclear translocation in WT MEFs treated with H₂O₂. Scale bar: 20 μ m. (B) Immunoblot analysis of EndoG in senescent MEFs. (C) Confocal microscopy images of EndoG nuclear translocation in senescent MEFs. Scale bar: 20 μ m. (D) Fluorescence intensity of nuclear-localized EndoG in senescent MEFs. (E) WB analysis of EndoG and AIF cellular localization in senescent MEFs. WCL, whole cell lysate. (F) Confocal microscopy images of AIF in *Pten*^{-/-} MEFs. Scale bar: 20 μ m. All values are presented as the mean \pm SEM. Multiple unpaired t-test was used in D. **p* < 0.05; ***p* < 0.01; ****p* < 0.001; ns, not significant.

Previous evidence demonstrates that cells depleted of EndoG release high levels of mtDNA outside the mitochondria without impacting the total mtDNA content and inducing apoptosis¹¹². Notably, EndoG downregulation in *WT* MEFs not only increased the amount of cytosolic mtDNA but also induced cellular senescence and promoted the upregulation of SASP genes (Fig. 15A-E). On top of that, analysis in the *Pten*^{-/-} MEFs model demonstrates that disruption of *Endog* boosted senescence and SASP production (Fig. 15F-H). Together, these results suggest that mtROS induces mtDNA release and EndoG translocation in senescent cells, thereby protecting mtDNA from degradation by this endonuclease.

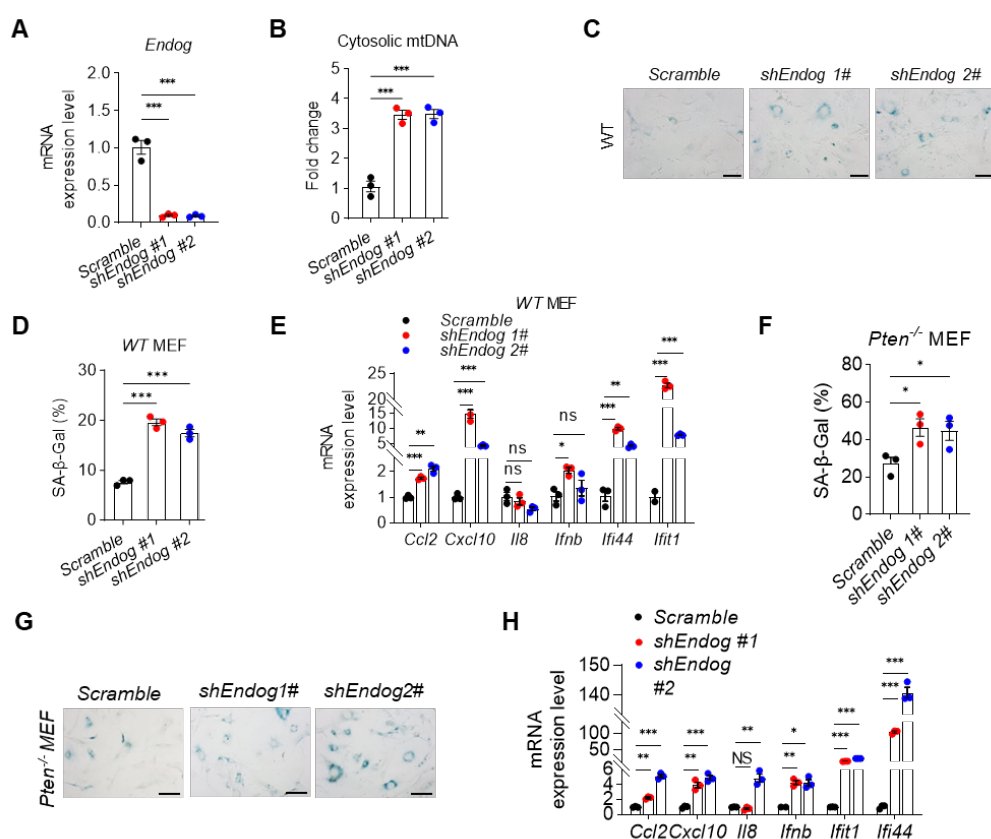


Fig 15. EndoG deficiency promotes mtDNA release and enhances senescence

(A) RT-qPCR of EndoG mRNA expression in WT MEFs infected with *shEndog* lentivirus. (B-D) qPCR analysis of cytosolic mtDNA (B), SA- β -gal staining image (C), and quantification (D) in WT MEFs infected with *shEndog* lentivirus. (E) Indicated SASP gene expression was detected in WT MEFs after *Endog* knocking down. (F-H) SA- β -gal staining quantification (F) and representative images (G) indicated SASP gene expression (H) in *Pten*^{-/-} MEFs infected with *shEndog* lentivirus. All values are presented as the mean \pm SEM. One-way ANOVA followed by Tukey's multiple comparisons test was used in A, B, and D-F. Multiple unpaired t-test was used in H. * $p < 0.05$; ** $p < 0.01$; *** $p < 0.001$; ns, not significant.

3.9 Senescent cells release mtDNA through VDAC

The effect of cytosolic mtDNA on SASP in senescent tumor cells and mtDNA-triggered immunosuppression in PMN-MDSC prompted us to think about the significance of mtDNA release blockage during cancer therapy. We next focused on the mechanism by which mtDNA is released outside the mitochondria. In apoptosis, mtDNA release is mediated by macropores in the mitochondrial outer membrane (MOM) created by oligomerization of the proteins BAX and BAK⁶⁸. In cells subjected to oxidative stress, mtDNA can escape through channels formed by mitochondrial permeability transition pores (mPTP) and oligomerizing voltage-dependent anion channels (VDAC1)^{68,112}. We therefore checked whether mtDNA release from senescent cells could be blocked by treatment with a BAX inhibitor (BAX Inhibiting Peptide V5, BIP-V5) and mPTP inhibitor (cyclosporin A, CsA). However, qPCR analysis performed in the cytosolic fraction of senescent cells showed no decrease in mtDNA release upon treatment with these compounds (Fig. 16A). We then investigated whether VDACs could mediate the cytosolic mtDNA release in senescent cells by knocking down *Vdac1* and *Vdac2* expression (Fig 16B). In *Pten*^{-/-} MEF, knocking down *Vdac1* or *Vdac2* significantly reduced both the cytosolic and extracellular release of mtDNA (Fig 16C, D). Consistent with the decreased mtDNA release, the *Vdac1* or *Vdac2* knocking down also reduced senescence and SASP gene expression in

PICS (Fig. 16E-H). A similar effect of *Vdac1* or *Vdac2* knocking down on senescence was also observed in OIS and TIS (Fig. 16I-K).

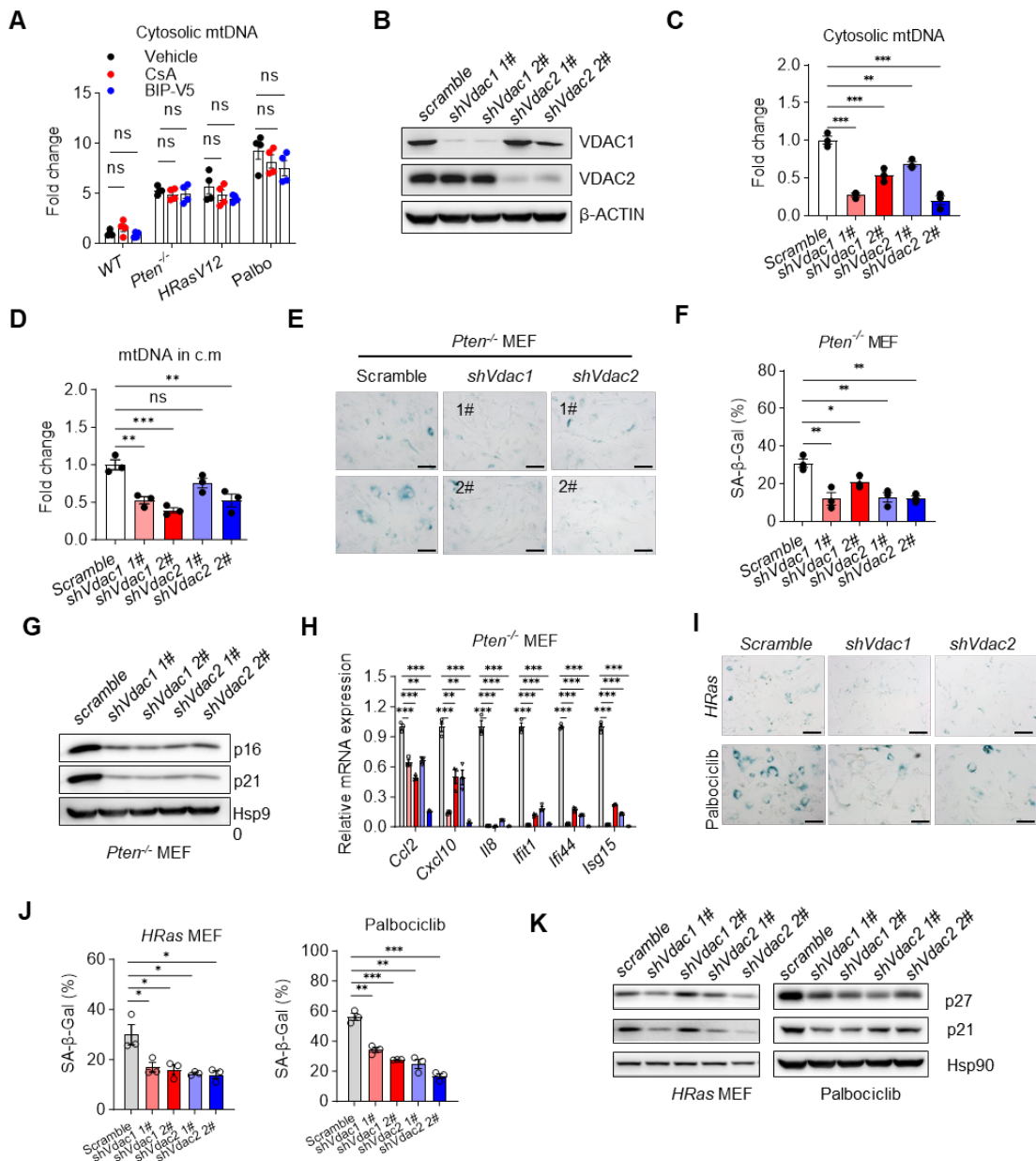


Fig 16. Cytosolic mtDNA releases in senescent cells occur through VDAC

(A) Quantification of cytosolic mtDNA in senescent MEFs treated with mPTP inhibitor CsA at 2.5 μ M and BAX inhibitor BIP-V5 at 10 μ M. (B) WB analysis of VDAC1 and VDAC2 in MEFs infected with *Scramble* or *shVdac1*, *shVdac2* lentivirus. (C and D) Quantification of mtDNA in the cytosol (C) and c.m (D) of *Pten*^{-/-} MEF infected *Scramble* or *shVdac1*, *shVdac2* lentivirus. (E and F) Quantification of SA- β -gal staining of *Pten*^{-/-} MEF infected with *Scramble* or *shVdac1*, *shVdac2* lentivirus. (G and H) WB analysis and RT-qPCR of indicated protein and

genes in *Pten*^{-/-} MEFs infected with *Scramble* or *shVdac1*, *shVdac2* lentivirus. (I-K) Representative images (I) and quantification (J) of SA-β-gal staining, and WB analysis of indicated proteins (K) in *HRas* and Palbociclib treated MEFs infected with *Scramble* or *shVdac1*, *shVdac2* lentivirus. All values are presented as the mean ± SEM. One-way ANOVA followed by Tukey's multiple comparisons test was used in A, C, D, F, and J. Multiple unpaired t-test was used in H. **p* < 0.05; ***p* < 0.01; ****p* < 0.001; ns, not significant.

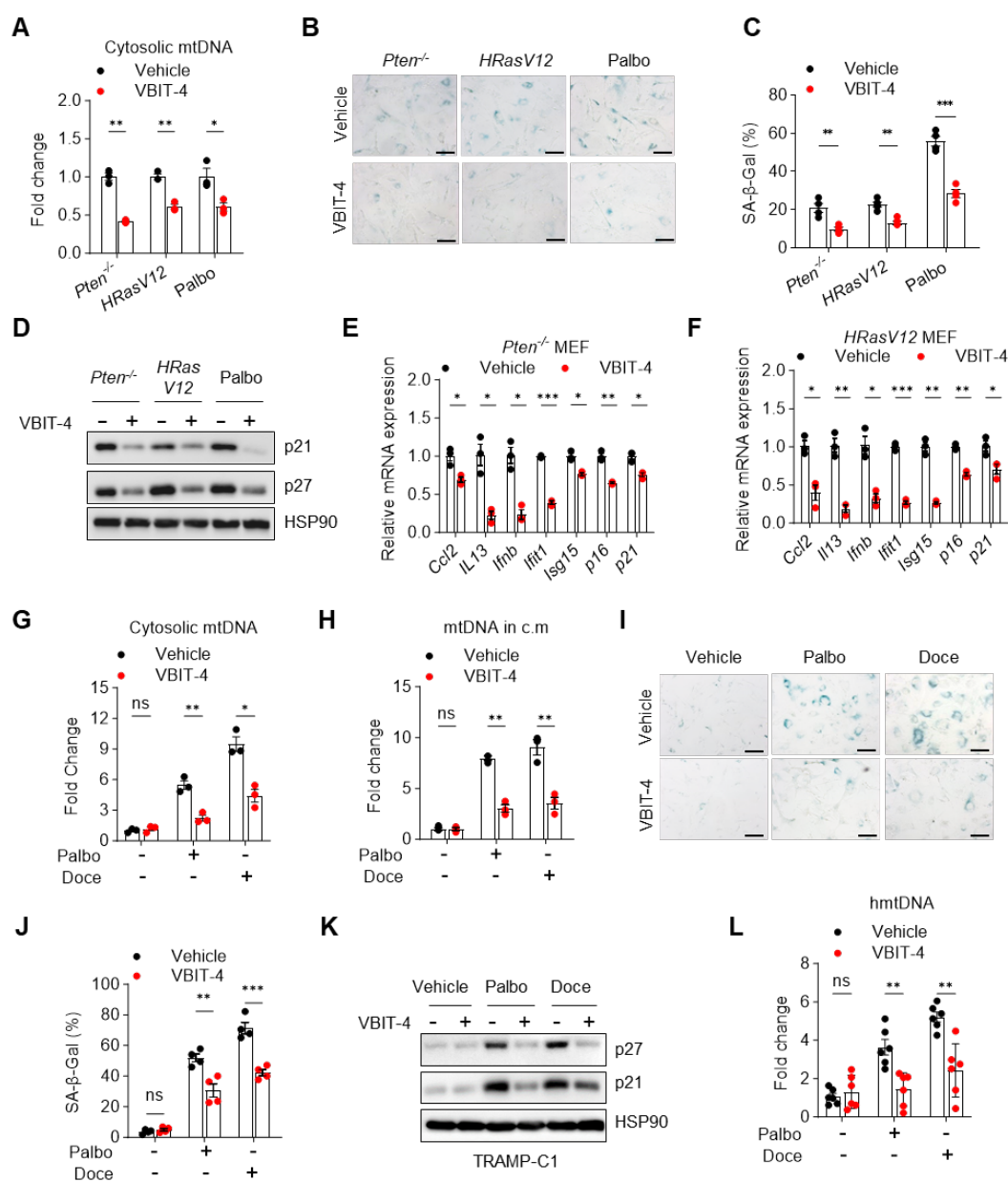


Fig 17. VDAC1 inhibitor blocks mtDNA release and senescence induction.

(A) Quantification of cytosolic mtDNA in senescent MEFs treated with VDAC1 inhibitor VBIT-4 at 5 μM. (B-D) SA-β-gal staining (B), quantification (C), indicated that protein (D) was detected in senescent MEFs treated with VBIT-4. (E and F) The expression of indicated genes in *Pten*^{-/-} (E) and *HRasV12* (F) MEFs treated with VBIT-4.

(G and H) Quantification of mtDNA in the cytosol (G) and c.m (H) of senescent TRAMP-C1 cells treated with VBIT-4 at 5 μ M. (I-K) SA- β -gal staining (I), quantification (J), and indicated protein (K) were detected in senescent TRAMP-C1 treated with VBIT-4. (L) qPCR analysis of human mtDNA in mouse BM-MDSC co-cultured with PC3 cells treated with Palbo or Doce combined w/o VBIT-4. All values are presented as the mean \pm SEM. Multiple unpaired t-test was used in A, C, E-H, J, and L. * $p < 0.05$; ** $p < 0.01$; *** $p < 0.001$; ns, not significant.

In addition, cells undergoing senescence treated by VBIT-4, a selective inhibitor of VDAC1 oligomerization, impaired the release of mtDNA in the cytosol (Fig. 17A). Consequently, VBIT-4 treatment interference in the establishment of cellular senescence and SASP production in senescent MEFs (Fig. 17B-F). Similarly, VBIT-4 blocked the release of mtDNA in the cytosol and culture media in the tumor cells with TIS (Fig. 17G-H), as well as cellular senescence (Fig. 17I-K). Inhibiting mtDNA release through VDAC1 inhibitor VBIT-4 in tumor cells also decreased the mtDNA uptake by murine BM-MDSCs (Fig. 17L). Taken together, our findings demonstrate that VDACS are involved in the release of mtDNA during cellular senescence and that pharmacological inhibition of VDAC in senescent cells may work as a therapeutic strategy to suppress the detrimental effect of the SASP in TIS ¹³.

3.10 Blockage of mtDNA release improves TIS efficacy

We next assessed whether blockage of extracellular mtDNA release in senescent cells could enhance the efficacy of Palbociclib treatment. Since VBIT4 treatment decreased the levels of mtDNA release in the cytosol and extracellular space of senescent cells, we hypothesized that this compound could work as both a senostatic by reducing the SASP and direct anti-inflammatory agent by affecting the activation of PMN-MDSCs in tumors treated with Palbociclib. First, we treated TRAMP-C1 tumor-bearing mice with Palbociclib to induce

senescence; next, we administered VBIT-4 to prevent the release of mtDNA and thereby inhibit the SASP and the simultaneous activation of PMN-MDSCs.

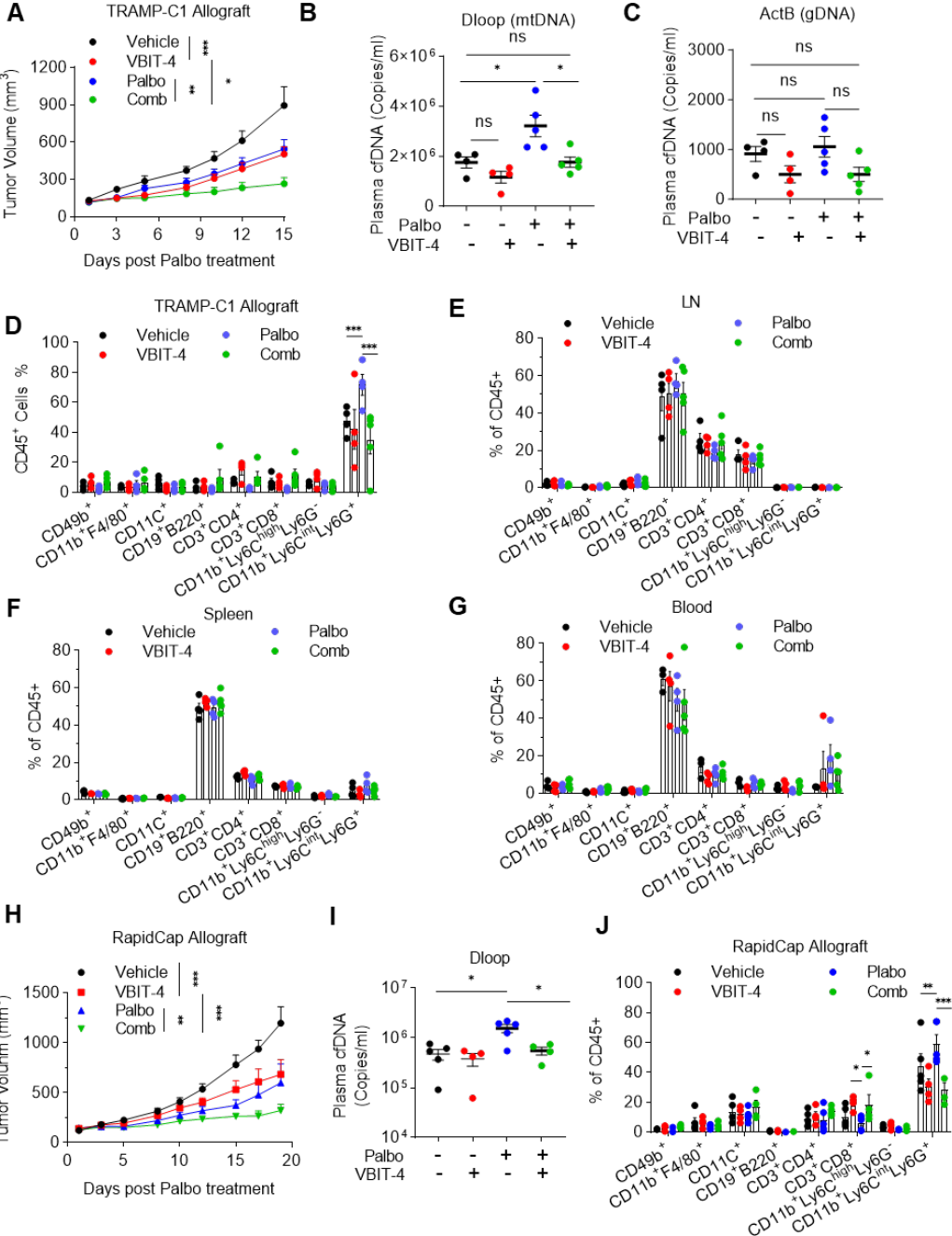


Fig 18. VBIT-4 treatment blocks mtDNA release, enhancing the efficacy of TIS.

(A) TRAMP-C1 tumor growth in mice with Palbo, VBIT-4, or combination treatment. UT: n=6, VBIT-4: n=5, Palbo: n=9, Comb: n=5. (B and C) Absolute quantification of plasma cell-free mtDNA (B) and nDNA (C) copy number in TRAMP-C1 tumor-bearing mice with Palbo, VBIT-4, or combination treatment. (D-G) Percentages of immune cell populations infiltration in the tumor (D), LN (E), spleen (F), and blood (G) (gated on CD45⁺ cells). (H) RapidCap tumor growth in mice with Palbo, VBIT-4, or combination treatment. UT: n=9, VBIT-4: n=6, Palbo:

n=7, Comb: n=7. (I) Absolute quantification of plasma cell-free mtDNA (Dloop) copy number in RapidCap tumor-bearing mice with Palbo, VBIT-4, or combination treatment. (J) Percentages of tumor-infiltrating immune cell populations (gated on CD45+ cells). All values are presented as the mean \pm SEM. Two-way ANOVA followed by Dunnett's multiple comparisons test was used to evaluate the statistical significance in A-J. *p < 0.05; **p < 0.01; ***p < 0.001; ns, not significant.

We found that VBIT-4 increased the efficacy of Palbociclib treatment by decreasing tumor size (Fig. 18A). Of note, Palbociclib increased the levels of mtDNA in the plasma of treated mice without affecting the levels of nDNA (Fig. 18b, C). However, VBIT-4 also decreased the frequency of intratumoral CD11b⁺Ly6G⁺Ly6C^{int} cells without affecting the number of these immune cell populations in the blood, spleen, and lymph node (Fig. 18D-G). These data were further validated in the RapidCap (PTEN/p53-deficient) allograft prostate tumor model, where Palbociclib was administered alone or combined with VBIT-4 (Fig. 18H-J).

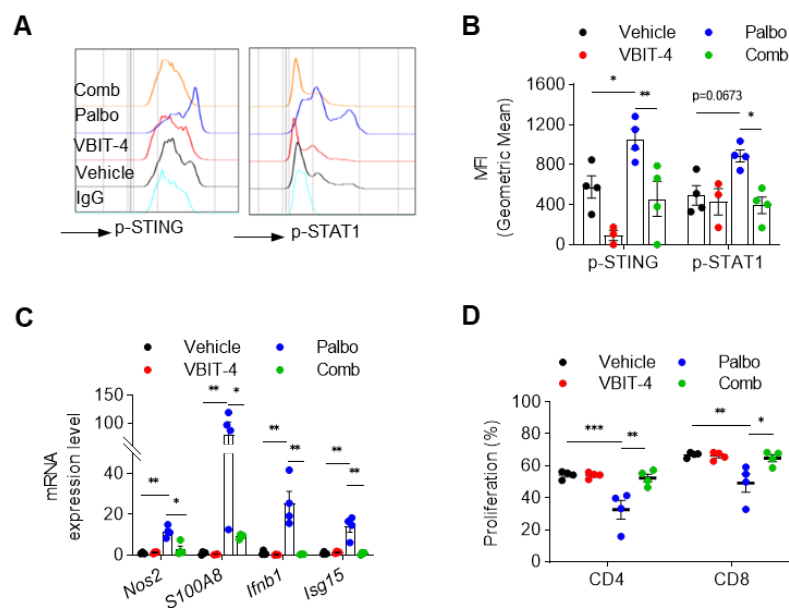


Fig 19. VBIT-4 treatment inhibits PMN-MDSC immunosuppressive function *in vivo*.

(A) Representative histogram of p-STING and p-STAT1 in CD11b⁺Ly6G⁺ PMN-MDSC sorted from TRAMP-C1 tumors with Palbo, VBIT-4, or combination treatment. (B) Fluorescence intensity of p-STING1 and p-STAT1 in CD11b⁺ Ly6G⁺ PMN-MDSC from TRAMP-C1 tumors as before. (C) RT-qPCR analysis of indicated genes in sorted PMN-MDSC as before. (D) Immunosuppressive activity by CD11b⁺ Ly6G⁺ PMN-MDSC sorted from TRAMP-C1 tumors as mentioned before. All values are presented as the mean \pm SEM. Two-way ANOVA followed by Dunnett's multiple comparisons test was used to evaluate the statistical significance in B-D. *p < 0.05; **p < 0.01; ***p < 0.001; ns, not significant.

We further sorted PMN-MDSCs from tumors treated with Palbo and VBIT-4. FACS analysis performed in these cells also showed reduced activation of the cGAS-STING pathway in MDSCs from mice treated with Palbo and VBIT-4 compared to Palbo-treated mice (Fig. 19A, B). We also detected a decreased expression of *iNOS2* and *S100A8* in line with the decreased immunosuppressive activity of these cells (Fig. 19C, D). These data demonstrate that the blockade of mtDNA release in TIS during prostate cancer therapy can reprogram tumor-infiltrating PMN-MDSCs, promoting the antitumor effects.

Discussion

Senescent cells accumulate in a variety of organs and tissues with age and different chronic diseases. Recently, it has been established that senescent cells can drive to a certain extent ageing and age-related pathologies⁵⁵, mainly by developing a complex SASP. Due to the disruption of the nuclear envelope integrity and DNA damage response (DDR), senescent cells release chromosome fragments into the cytoplasm, which activate the cGAS-STING pathway and appear to underlie key SASP. Previous research has demonstrated that CCF could accumulate in the cytoplasm and activate cytoplasmic pro-inflammatory pathways in senescence and cancer^{63,94}. Thus, cellular senescence reflects the axis of genome instability, misplaced cytosolic self-DNA, and inflammation, in the aging process. Moreover, in senescent cells, genomic retrotransposable elements (TE) and endogenous retrovirus (ERV) sequences become transcriptionally activated and could be reverse-transcribed to cDNA in the cytosol. The increased cytosolic LINE-1 and ERV cDNA become a source of cGAS-STING activation in senescent cells^{64,65,113}. These studies indicate the diverse resources of cytosolic DNA.

Mitochondria, an essential mediator of inflammation and the SASP in both ageing and the development of the senescent phenotype^{39,51,113}, also contains its DNA (mtDNA) that can be released into the cytosol triggered by different stress, such as infection and cell death^{68,70,114}. Recently, mtDNA has also been reported to be released into the cytosol in senescent cells induced by radiation through BAX/BAK⁷⁴. Cytosolic mtDNA in turn activates the cGAS-STING pathway to regulate the SASP. However, these cytosolic DNA stimuli are studied when the senescence has been established. Whether this DNA is released to cytosol during the early stage of senescence and regulates senescence induction is unknown. Here, we have demonstrated that cytosolic mtDNA release is essential in the initial stage during senescence induction across various senescent models, a previously unknown finding. By time points experiment, we found mtDNA released to cytosol even at the beginning of senescence induction.

Of note, the mtDNA release also precedes nuclear DNA in OIS. It highlights the importance of mtDNA than nDNA during senescence induction.

DNA localization in the cytoplasm of a cell, whether exogenous or endogenous, acts as a potent danger signal that stimulates an innate immune response. Our investigation reveals that mtDNA released by senescent tumor cells enters the extracellular space via extracellular vesicles (EVs). Senescent cells are reported to exhibit an increased secretion of EVs. We further confirmed that the EVs released by senescent cells contain a higher concentration of mtDNA compared to the EVs derived from non-senescent cells. In the tumor microenvironment, senescent tumor cells have been observed to release extracellular mitochondrial DNA (mtDNA), which is selectively taken up by PMN-MDSCs but not by DCs and macrophages. Our investigations have provided evidence indicating that PMN-MDSCs exhibit a superior capacity for the uptake of senescent cell-derived EVs, both in *in vivo* and *in vitro* settings. However, the underlying mechanisms governing this preferential uptake remain to be fully elucidated. Further study is required to unravel the pathways involved in this process.

The internalization of mtDNA by PMN-MDSC leads to the activation of the cGAS-STING pathway that enhances the immune suppressive ability of these cells, thereby promoting tumor immune suppression. Notably, the activation of the cGAS/STING pathway in the tumor microenvironment can induce the effective cross-priming of tumor-specific antigens and promote the infiltration of effector T cells¹¹⁵. Consequently, several STING agonists have been developed for clinical trials to simulate this activation, aiming to bolster the anticancer immune response. However, it is essential to acknowledge that chronic STING activation may lead to a protumor phenotype in certain malignancies^{116,117}. A previous paper demonstrates that STING activation in regulatory B cells through a STING agonist enhances the immune suppression capability of these immune cells¹¹⁷. Given that the activation of the cGAS-STING pathway in PMN-MDSCs contributes to tumor immune suppression, and PMN-MDSC is the main myeloid

immune population in prostate cancer, further research will be required to obtain a more in-depth knowledge of the STING-related tumor microenvironment to reveal the potential effect of STING agonist therapy in prostate cancer. STING activation triggers multiple signaling cascades, inducing both type I interferon (IFN) expression and NF- κ B-mediated cytokine production. The immuno-suppressive activity of MDSCs in cancer has been reported to require inactivation of the type I interferon pathway^{103,118}. Notably, we found that MDSCs showed a lower capacity of type I interferon response compared to DCs and macrophages upon cGAS-STING activation. Meanwhile, the enhanced immunosuppression in BM-MDSCs upon mtDNA treatment mainly relies on the activation of the cGAS-STING-NF- κ B pathway. Consequently, unraveling the mechanisms underlying this phenomenon and identifying the regulators that modulate the two branches of the STING downstream pathway will be imperative for future translational applications. Understanding these intricacies holds significant promise for refining therapeutic strategies aimed at mitigating immunosuppression within the tumor microenvironment.

Furthermore, our study has also elucidated the intricate mechanisms underlying the release of mtDNA. Specifically, we have delineated a process whereby nuclear translocation of EndoG, distinct from AIF, facilitates the escape of damaged mtDNA from degradation by this endonuclease. Subsequently, the mtDNA bypasses the mitochondrial membranes through VDACs. Victorelli, S. *et al.* find that mitochondrial outer membrane permeabilization (MOMP) occurs in a subset of mitochondria in senescent cells induced by apoptotic stress⁷⁴. This process, called minority MOMP (miMOMP), requires BAX and BAK macropores, enabling the release of mtDNA into the cytosol. BAX and BAK accumulate in the mitochondrial outer membrane in response to apoptotic stimuli, leading to the release of cytochrome C, which initiates the apoptotic cascade in cytosol¹¹⁹. In our work, we found that the mtDNA release in senescent cells was not changed upon BAX/BAK inhibitor treatment, which indicates that this process,

at least in PICS, OIS, and TIS, is BAX/BAK independent. This can be explained by the senescence models we used were induced by non-lethal stress, which is more cancer-relevant. Supporting this hypothesis, we also did not observe the activation of Caspase 3 and the change of Annexin V staining in our senescence models. In conclusion, we propose that the MOM pore that mediates mtDNA release and SASP depends on the level of mitochondrial stress: oligomerized VDAC1 for moderate-level stress and BAX/BAK macropores for extreme-level stress and/or apoptosis.

This elucidation of the molecular machinery involved in mtDNA release adds depth to our understanding of cellular responses to mitochondrial dysfunction and may hold implications for the development of targeted therapeutic interventions aimed at modulating mtDNA-mediated processes in various pathological contexts. Remarkably, pharmacological inhibition of VDAC1 oligomerization using VBIT-4 significantly reduced the release of cytosolic mtDNA and SASP factors from senescent cells. This highlights the potential of this compound as a senostatic drug in cancer therapy. Furthermore, VBIT-4 treatment also reduces the extracellular pool of mtDNA, resulting in a significant decrease in the uptake of extracellular mtDNA by PMN-MDSCs, consistent with the blockage of cytosolic mtDNA release. Decreased mtDNA release, in turn, enhanced the efficacy of chemotherapy by alleviating immunosuppression in the TME. Nevertheless, inhibiting VDAC oligomerization may be an alternate therapeutic approach for a wide range of diseases, like SLE and Parkinson's disease, which are associated with mtDNA release.

Collectively, our work provides novel insights into senescence, highlighting the dual role of accumulated senescent cell-associated mtDNA as an intracellular and extracellular signal molecule. These mechanistic insights shed new light on how senescent cells-derived mtDNA engages senescence and inflammatory responses in cancer. These findings suggest that blocking mtDNA release in TIS holds great potential as a promising therapeutic strategy to

enhance the efficacy of chemotherapy in clinical cancer treatment. Furthermore, the implications extend beyond cancer therapy, as inhibiting VDAC oligomerization presents a potential therapeutic approach for a wide spectrum of diseases, such as systemic lupus erythematosus (SLE) and Parkinson's disease, both of which are associated with aberrant mtDNA release. The multifaceted impact of VBIT-4 underscores its potential as a versatile therapeutic agent with implications across diverse pathological conditions, offering new avenues for targeted intervention and disease management.

Reference

- 1 Calcinotto, A. *et al.* IL-23 secreted by myeloid cells drives castration-resistant prostate cancer. *Nature*, doi:10.1038/s41586-018-0266-0 (2018).
- 2 Demaria, M. *et al.* Cellular Senescence Promotes Adverse Effects of Chemotherapy and Cancer Relapse. *Cancer Discovery* **7**, 165-176, doi:10.1158/2159-8290.cd-16-0241 (2017).
- 3 Serrano, M., Lin, A. W., McCurrach, M. E., Beach, D. & Lowe, S. W. Oncogenic ras provokes premature cell senescence associated with accumulation of p53 and p16INK4a. *Cell* **88**, 593-602, doi:10.1016/s0092-8674(00)81902-9 (1997).
- 4 Sarkisian, C. J. *et al.* Dose-dependent oncogene-induced senescence in vivo and its evasion during mammary tumorigenesis. *Nat Cell Biol* **9**, 493-505, doi:10.1038/ncb1567 (2007).
- 5 Wyld, L. *et al.* Senescence and Cancer: A Review of Clinical Implications of Senescence and Senotherapies. *Cancers (Basel)* **12**, doi:10.3390/cancers12082134 (2020).
- 6 Collado, M. *et al.* Tumour biology: senescence in premalignant tumours. *Nature* **436**, 642, doi:10.1038/436642a (2005).
- 7 Huang, W., Hickson, L. J., Eirin, A., Kirkland, J. L. & Lerman, L. O. Cellular senescence: the good, the bad and the unknown. *Nat Rev Nephrol* **18**, 611-627, doi:10.1038/s41581-022-00601-z (2022).
- 8 Liu, X. L., Ding, J. & Meng, L. H. Oncogene-induced senescence: a double edged sword in cancer. *Acta Pharmacol Sin* **39**, 1553-1558, doi:10.1038/aps.2017.198 (2018).
- 9 Lee, J. J. *et al.* PTEN status switches cell fate between premature senescence and apoptosis in glioma exposed to ionizing radiation. *Cell Death Differ* **18**, 666-677, doi:10.1038/cdd.2010.139 (2011).
- 10 Alimonti, A. *et al.* A novel type of cellular senescence that can be enhanced in mouse

- models and human tumor xenografts to suppress prostate tumorigenesis. *Journal of Clinical Investigation* **120**, 681-693, doi:10.1172/jci40535 (2010).
- 11 Augello, G. *et al.* A PTEN inhibitor displays preclinical activity against hepatocarcinoma cells. *Cell Cycle* **15**, 573-583, doi:10.1080/15384101.2016.1138183 (2016).
- 12 Chen, Z. *et al.* Crucial role of p53-dependent cellular senescence in suppression of Pten-deficient tumorigenesis. *Nature* **436**, 725-730, doi:10.1038/nature03918 (2005).
- 13 Wang, L., Lankhorst, L. & Bernards, R. Exploiting senescence for the treatment of cancer. *Nat Rev Cancer* **22**, 340-355, doi:10.1038/s41568-022-00450-9 (2022).
- 14 Lee, M. & Lee, J. S. Exploiting tumor cell senescence in anticancer therapy. *BMB Rep* **47**, 51-59, doi:10.5483/bmbrep.2014.47.2.005 (2014).
- 15 d'Adda di Fagagna, F. *et al.* A DNA damage checkpoint response in telomere-initiated senescence. *Nature* **426**, 194-198, doi:10.1038/nature02118 (2003).
- 16 Schmitt, C. A. *et al.* A senescence program controlled by p53 and p16INK4a contributes to the outcome of cancer therapy. *Cell* **109**, 335-346, doi:10.1016/s0092-8674(02)00734-1 (2002).
- 17 Revandkar, A. *et al.* Inhibition of Notch pathway arrests PTEN-deficient advanced prostate cancer by triggering p27-driven cellular senescence. *Nature Communications* **7**, 13719, doi:10.1038/ncomms13719 (2016).
- 18 Kalathur, M. *et al.* A chemogenomic screening identifies CK2 as a target for pro-senescence therapy in PTEN-deficient tumours. *Nature Communications* **6**, doi:10.1038/ncomms8227 (2015).
- 19 Goel, S. *et al.* CDK4/6 inhibition triggers anti-tumour immunity. *Nature* **548**, 471-475, doi:10.1038/nature23465 (2017).
- 20 Prata, L., Ovsyannikova, I. G., Tchkonja, T. & Kirkland, J. L. Senescent cell clearance

- by the immune system: Emerging therapeutic opportunities. *Semin Immunol* **40**, 101275, doi:10.1016/j.smim.2019.04.003 (2018).
- 21 Coppe, J. P., Desprez, P. Y., Krtolica, A. & Campisi, J. The senescence-associated secretory phenotype: the dark side of tumor suppression. *Annu Rev Pathol* **5**, 99-118, doi:10.1146/annurev-pathol-121808-102144 (2010).
- 22 Kuilman, T. *et al.* Oncogene-induced senescence relayed by an interleukin-dependent inflammatory network. *Cell* **133**, 1019-1031, doi:10.1016/j.cell.2008.03.039 (2008).
- 23 Ortiz-Montero, P., Londono-Vallejo, A. & Vernot, J. P. Senescence-associated IL-6 and IL-8 cytokines induce a self- and cross-reinforced senescence/inflammatory milieu strengthening tumorigenic capabilities in the MCF-7 breast cancer cell line. *Cell Commun Signal* **15**, 17, doi:10.1186/s12964-017-0172-3 (2017).
- 24 Acosta, J. C. *et al.* A complex secretory program orchestrated by the inflammasome controls paracrine senescence. *Nat Cell Biol* **15**, 978-990, doi:10.1038/ncb2784 (2013).
- 25 Baker, D. J. *et al.* Clearance of p16Ink4a-positive senescent cells delays ageing-associated disorders. *Nature* **479**, 232-236, doi:10.1038/nature10600 (2011).
- 26 Marin, I., Serrano, M. & Pietrocola, F. Recent insights into the crosstalk between senescent cells and CD8 T lymphocytes. *NPJ Aging* **9**, 8, doi:10.1038/s41514-023-00105-5 (2023).
- 27 Lujambio, A. *et al.* Non-cell-autonomous tumor suppression by p53. *Cell* **153**, 449-460, doi:10.1016/j.cell.2013.03.020 (2013).
- 28 Kang, T. W. *et al.* Senescence surveillance of pre-malignant hepatocytes limits liver cancer development. *Nature* **479**, 547-551, doi:10.1038/nature10599 (2011).
- 29 Krtolica, A., Parrinello, S., Lockett, S., Desprez, P. Y. & Campisi, J. Senescent fibroblasts promote epithelial cell growth and tumorigenesis: a link between cancer and aging. *Proc Natl Acad Sci USA* **98**, 12072-12077, doi:10.1073/pnas.211053698 (2001).

- 30 Coppe, J. P., Kauser, K., Campisi, J. & Beausejour, C. M. Secretion of vascular endothelial growth factor by primary human fibroblasts at senescence. *J Biol Chem* **281**, 29568-29574, doi:10.1074/jbc.M603307200 (2006).
- 31 Bavik, C. *et al.* The gene expression program of prostate fibroblast senescence modulates neoplastic epithelial cell proliferation through paracrine mechanisms. *Cancer Res* **66**, 794-802, doi:10.1158/0008-5472.CAN-05-1716 (2006).
- 32 Ruhland, M. K. *et al.* Stromal senescence establishes an immunosuppressive microenvironment that drives tumorigenesis. *Nat Commun* **7**, 11762, doi:10.1038/ncomms11762 (2016).
- 33 Di Mitri, D. *et al.* Tumour-infiltrating Gr-1+ myeloid cells antagonize senescence in cancer. *Nature* **515**, 134-137, doi:10.1038/nature13638 (2014).
- 34 Eggert, T. *et al.* Distinct Functions of Senescence-Associated Immune Responses in Liver Tumor Surveillance and Tumor Progression. *Cancer Cell* **30**, 533-547, doi:10.1016/j.ccell.2016.09.003 (2016).
- 35 Desdin-Mico, G. *et al.* T cells with dysfunctional mitochondria induce multimorbidity and premature senescence. *Science* **368**, 1371-1376, doi:10.1126/science.aax0860 (2020).
- 36 Montes, C. L. *et al.* Tumor-induced senescent T cells with suppressor function: a potential form of tumor immune evasion. *Cancer Res* **68**, 870-879, doi:10.1158/0008-5472.CAN-07-2282 (2008).
- 37 Guccini, I. *et al.* Senescence Reprogramming by TIMP1 Deficiency Promotes Prostate Cancer Metastasis. *Cancer Cell* **39**, 68-82 e69, doi:10.1016/j.ccell.2020.10.012 (2021).
- 38 Correia-Melo, C. & Passos, J. F. Mitochondria: Are they causal players in cellular senescence? *Biochim Biophys Acta* **1847**, 1373-1379, doi:10.1016/j.bbabi.2015.05.017 (2015).

- 39 Moiseeva, O., Bourdeau, V., Roux, A., Deschenes-Simard, X. & Ferbeyre, G. Mitochondrial dysfunction contributes to oncogene-induced senescence. *Mol Cell Biol* **29**, 4495-4507, doi:10.1128/MCB.01868-08 (2009).
- 40 Passos, J. F. *et al.* Mitochondrial dysfunction accounts for the stochastic heterogeneity in telomere-dependent senescence. *PLoS Biol* **5**, e110, doi:10.1371/journal.pbio.0050110 (2007).
- 41 Kaplon, J. *et al.* A key role for mitochondrial gatekeeper pyruvate dehydrogenase in oncogene-induced senescence. *Nature* **498**, 109-112, doi:10.1038/nature12154 (2013).
- 42 Korolchuk, V. I., Miwa, S., Carroll, B. & von Zglinicki, T. Mitochondria in Cell Senescence: Is Mitophagy the Weakest Link? *EBioMedicine* **21**, 7-13, doi:10.1016/j.ebiom.2017.03.020 (2017).
- 43 Lee, H. C., Yin, P. H., Chi, C. W. & Wei, Y. H. Increase in mitochondrial mass in human fibroblasts under oxidative stress and during replicative cell senescence. *J Biomed Sci* **9**, 517-526, doi:10.1007/BF02254978 (2002).
- 44 Yoon, Y. S. *et al.* Formation of elongated giant mitochondria in DFO-induced cellular senescence: involvement of enhanced fusion process through modulation of Fis1. *J Cell Physiol* **209**, 468-480, doi:10.1002/jcp.20753 (2006).
- 45 Lee, S. *et al.* Mitochondrial fission and fusion mediators, hFis1 and OPA1, modulate cellular senescence. *J Biol Chem* **282**, 22977-22983, doi:10.1074/jbc.M700679200 (2007).
- 46 Garcia-Prat, L. *et al.* Autophagy maintains stemness by preventing senescence. *Nature* **529**, 37-42, doi:10.1038/nature16187 (2016).
- 47 Rizza, S. *et al.* S-nitrosylation drives cell senescence and aging in mammals by controlling mitochondrial dynamics and mitophagy. *Proc Natl Acad Sci U S A* **115**, E3388-E3397, doi:10.1073/pnas.1722452115 (2018).

- 48 Ahmad, T. *et al.* Impaired mitophagy leads to cigarette smoke stress-induced cellular senescence: implications for chronic obstructive pulmonary disease. *FASEB J* **29**, 2912-2929, doi:10.1096/fj.14-268276 (2015).
- 49 Hoshino, A. *et al.* Cytosolic p53 inhibits Parkin-mediated mitophagy and promotes mitochondrial dysfunction in the mouse heart. *Nat Commun* **4**, 2308, doi:10.1038/ncomms3308 (2013).
- 50 Manzella, N. *et al.* Monoamine oxidase-A is a novel driver of stress-induced premature senescence through inhibition of parkin-mediated mitophagy. *Aging Cell* **17**, e12811, doi:10.1111/accel.12811 (2018).
- 51 Wiley, C. D. *et al.* Mitochondrial Dysfunction Induces Senescence with a Distinct Secretory Phenotype. *Cell Metab* **23**, 303-314, doi:10.1016/j.cmet.2015.11.011 (2016).
- 52 Miwa, S., Kashyap, S., Chini, E. & von Zglinicki, T. Mitochondrial dysfunction in cell senescence and aging. *J Clin Invest* **132**, doi:10.1172/JCI158447 (2022).
- 53 Nacarelli, T. *et al.* NAD(+) metabolism governs the proinflammatory senescence-associated secretome. *Nat Cell Biol* **21**, 397-407, doi:10.1038/s41556-019-0287-4 (2019).
- 54 Wang, W., Yang, X., Lopez de Silanes, I., Carling, D. & Gorospe, M. Increased AMP:ATP ratio and AMP-activated protein kinase activity during cellular senescence linked to reduced HuR function. *J Biol Chem* **278**, 27016-27023, doi:10.1074/jbc.M300318200 (2003).
- 55 Ogrodnik, M. *et al.* Cellular senescence drives age-dependent hepatic steatosis. *Nat Commun* **8**, 15691, doi:10.1038/ncomms15691 (2017).
- 56 Saretzki, G., Murphy, M. P. & von Zglinicki, T. MitoQ counteracts telomere shortening and elongates lifespan of fibroblasts under mild oxidative stress. *Aging Cell* **2**, 141-143, doi:10.1046/j.1474-9728.2003.00040.x (2003).

- 57 Passos, J. F. *et al.* Feedback between p21 and reactive oxygen production is necessary for cell senescence. *Mol Syst Biol* **6**, 347, doi:10.1038/msb.2010.5 (2010).
- 58 Martini, H. & Passos, J. F. Cellular senescence: all roads lead to mitochondria. *FEBS J* **290**, 1186-1202, doi:10.1111/febs.16361 (2023).
- 59 Zwerschke, W. *et al.* Metabolic analysis of senescent human fibroblasts reveals a role for AMP in cellular senescence. *Biochem J* **376**, 403-411, doi:10.1042/BJ20030816 (2003).
- 60 Shimada, K. *et al.* Oxidized mitochondrial DNA activates the NLRP3 inflammasome during apoptosis. *Immunity* **36**, 401-414, doi:10.1016/j.immuni.2012.01.009 (2012).
- 61 Zhou, R., Yazdi, A. S., Menu, P. & Tschopp, J. A role for mitochondria in NLRP3 inflammasome activation. *Nature* **469**, 221-225, doi:10.1038/nature09663 (2011).
- 62 West, A. P. *et al.* Mitochondrial DNA stress primes the antiviral innate immune response. *Nature* **520**, 553-557, doi:10.1038/nature14156 (2015).
- 63 Dou, Z. *et al.* Cytoplasmic chromatin triggers inflammation in senescence and cancer. *Nature* **550**, 402-406, doi:10.1038/nature24050 (2017).
- 64 De Cecco, M. *et al.* L1 drives IFN in senescent cells and promotes age-associated inflammation. *Nature* **566**, 73-78, doi:10.1038/s41586-018-0784-9 (2019).
- 65 Liu, X. *et al.* Resurrection of endogenous retroviruses during aging reinforces senescence. *Cell* **186**, 287-304 e226, doi:10.1016/j.cell.2022.12.017 (2023).
- 66 Yum, S., Li, M., Fang, Y. & Chen, Z. J. TBK1 recruitment to STING activates both IRF3 and NF-kappaB that mediate immune defense against tumors and viral infections. *Proc Natl Acad Sci U S A* **118**, doi:10.1073/pnas.2100225118 (2021).
- 67 Yakes, F. M. & Van Houten, B. Mitochondrial DNA damage is more extensive and persists longer than nuclear DNA damage in human cells following oxidative stress. *Proc Natl Acad Sci U S A* **94**, 514-519, doi:10.1073/pnas.94.2.514 (1997).

- 68 McArthur, K. *et al.* BAK/BAX macropores facilitate mitochondrial herniation and mtDNA efflux during apoptosis. *Science* **359**, doi:10.1126/science.aao6047 (2018).
- 69 Riley, J. S. *et al.* Mitochondrial inner membrane permeabilisation enables mtDNA release during apoptosis. *EMBO J* **37**, doi:10.15252/emj.201899238 (2018).
- 70 Sun, B. *et al.* Dengue virus activates cGAS through the release of mitochondrial DNA. *Sci Rep* **7**, 3594, doi:10.1038/s41598-017-03932-1 (2017).
- 71 Ni, G., Ma, Z. & Damania, B. cGAS and STING: At the intersection of DNA and RNA virus-sensing networks. *PLoS Pathog* **14**, e1007148, doi:10.1371/journal.ppat.1007148 (2018).
- 72 Miller, K. N. *et al.* Cytoplasmic DNA: sources, sensing, and role in aging and disease. *Cell* **184**, 5506-5526, doi:10.1016/j.cell.2021.09.034 (2021).
- 73 White, M. J. *et al.* Apoptotic caspases suppress mtDNA-induced STING-mediated type I IFN production. *Cell* **159**, 1549-1562, doi:10.1016/j.cell.2014.11.036 (2014).
- 74 Victorelli, S. *et al.* Apoptotic stress causes mtDNA release during senescence and drives the SASP. *Nature*, doi:10.1038/s41586-023-06621-4 (2023).
- 75 Hajizadeh, S., DeGroot, J., TeKoppele, J. M., Tarkowski, A. & Collins, L. V. Extracellular mitochondrial DNA and oxidatively damaged DNA in synovial fluid of patients with rheumatoid arthritis. *Arthritis Res Ther* **5**, R234-240, doi:10.1186/ar787 (2003).
- 76 Ryu, C. *et al.* Extracellular Mitochondrial DNA Is Generated by Fibroblasts and Predicts Death in Idiopathic Pulmonary Fibrosis. *Am J Respir Crit Care Med* **196**, 1571-1581, doi:10.1164/rccm.201612-2480OC (2017).
- 77 Gong, T., Liu, L., Jiang, W. & Zhou, R. DAMP-sensing receptors in sterile inflammation and inflammatory diseases. *Nat Rev Immunol* **20**, 95-112, doi:10.1038/s41577-019-0215-7 (2020).

- 78 Huang, L. S. *et al.* mtDNA Activates cGAS Signaling and Suppresses the YAP-Mediated Endothelial Cell Proliferation Program to Promote Inflammatory Injury. *Immunity* **52**, 475-486 e475, doi:10.1016/j.immuni.2020.02.002 (2020).
- 79 Yu, C. H. *et al.* TDP-43 Triggers Mitochondrial DNA Release via mPTP to Activate cGAS/STING in ALS. *Cell* **183**, 636-649 e618, doi:10.1016/j.cell.2020.09.020 (2020).
- 80 Chung, K. W. *et al.* Mitochondrial Damage and Activation of the STING Pathway Lead to Renal Inflammation and Fibrosis. *Cell Metab* **30**, 784-799 e785, doi:10.1016/j.cmet.2019.08.003 (2019).
- 81 Zhang, Q. *et al.* Circulating mitochondrial DAMPs cause inflammatory responses to injury. *Nature* **464**, 104-107, doi:10.1038/nature08780 (2010).
- 82 Lam, L. K. M. *et al.* DNA binding to TLR9 expressed by red blood cells promotes innate immune activation and anemia. *Sci Transl Med* **13**, eabj1008, doi:10.1126/scitranslmed.abj1008 (2021).
- 83 Toso, A. *et al.* Enhancing Chemotherapy Efficacy in Pten -Deficient Prostate Tumors by Activating the Senescence-Associated Antitumor Immunity. *Cell Reports* **9**, 75-89, doi:10.1016/j.celrep.2014.08.044 (2014).
- 84 Munoz, D. P. *et al.* Targetable mechanisms driving immunoevasion of persistent senescent cells link chemotherapy-resistant cancer to aging. *JCI Insight* **5**, doi:10.1172/jci.insight.124716 (2019).
- 85 Solito, S. *et al.* Methods to Measure MDSC Immune Suppressive Activity In Vitro and In Vivo. *Curr Protoc Immunol* **124**, e61, doi:10.1002/cpim.61 (2019).
- 86 Sauter, M. *et al.* Protocol to isolate and analyze mouse bone marrow derived dendritic cells (BMDC). *STAR Protoc* **3**, 101664, doi:10.1016/j.xpro.2022.101664 (2022).
- 87 Toda, G., Yamauchi, T., Kadowaki, T. & Ueki, K. Preparation and culture of bone marrow-derived macrophages from mice for functional analysis. *STAR Protoc* **2**,

- 100246, doi:10.1016/j.xpro.2020.100246 (2021).
- 88 Frezza, C., Cipolat, S. & Scorrano, L. Organelle isolation: functional mitochondria from mouse liver, muscle and cultured fibroblasts. *Nat Protoc* **2**, 287-295, doi:10.1038/nprot.2006.478 (2007).
- 89 Dobin, A. *et al.* STAR: ultrafast universal RNA-seq aligner. *Bioinformatics* **29**, 15-21, doi:10.1093/bioinformatics/bts635 (2013).
- 90 Wu, D. & Smyth, G. K. Camera: a competitive gene set test accounting for inter-gene correlation. *Nucleic Acids Res* **40**, e133, doi:10.1093/nar/gks461 (2012).
- 91 Palmbos, P. L. *et al.* Clinical outcomes and markers of treatment response in a randomized phase II study of androgen deprivation therapy with or without palbociclib in RB-intact metastatic hormone-sensitive prostate cancer (mHSPC). *J Clin Oncol* **38** (2020).
- 92 Palmbos, P. L. *et al.* A Randomized Phase II Study of Androgen Deprivation Therapy with or without Palbociclib in RB-positive Metastatic Hormone-Sensitive Prostate Cancer. *Clin Cancer Res* **27**, 3017-3027, doi:10.1158/1078-0432.Ccr-21-0024 (2021).
- 93 Spadafora, D., Kozhukhar, N., Chouljenko, V. N., Kousoulas, K. G. & Alexeyev, M. F. Methods for Efficient Elimination of Mitochondrial DNA from Cultured Cells. *PLoS One* **11**, e0154684, doi:10.1371/journal.pone.0154684 (2016).
- 94 Gluck, S. *et al.* Innate immune sensing of cytosolic chromatin fragments through cGAS promotes senescence. *Nat Cell Biol* **19**, 1061-1070, doi:10.1038/ncb3586 (2017).
- 95 Wang, G. *et al.* Targeting YAP-Dependent MDSC Infiltration Impairs Tumor Progression. *Cancer Discov* **6**, 80-95, doi:10.1158/2159-8290.CD-15-0224 (2016).
- 96 Borghesan, M. *et al.* Small Extracellular Vesicles Are Key Regulators of Non-cell Autonomous Intercellular Communication in Senescence via the Interferon Protein IFITM3. *Cell Rep* **27**, 3956-3971 e3956, doi:10.1016/j.celrep.2019.05.095 (2019).

- 97 Meng, Q. *et al.* Surfaceome analysis of extracellular vesicles from senescent cells uncovers uptake repressor DPP4. *Proc Natl Acad Sci U S A* **120**, e2219801120, doi:10.1073/pnas.2219801120 (2023).
- 98 Xu, M. M. *et al.* Dendritic Cells but Not Macrophages Sense Tumor Mitochondrial DNA for Cross-priming through Signal Regulatory Protein alpha Signaling. *Immunity* **47**, 363-373 e365, doi:10.1016/j.immuni.2017.07.016 (2017).
- 99 Canton, J. Phagosome maturation in polarized macrophages. *J Leukoc Biol* **96**, 729-738, doi:10.1189/jlb.1MR0114-021R (2014).
- 100 Kim, J. H., Lee, C. H. & Baek, M. C. Dissecting exosome inhibitors: therapeutic insights into small-molecule chemicals against cancer. *Exp Mol Med* **54**, 1833-1843, doi:10.1038/s12276-022-00898-7 (2022).
- 101 Weber, R. *et al.* IL-6 as a major regulator of MDSC activity and possible target for cancer immunotherapy. *Cell Immunol* **359**, 104254, doi:10.1016/j.cellimm.2020.104254 (2021).
- 102 Veglia, F., Sanseviero, E. & Gabrilovich, D. I. Myeloid-derived suppressor cells in the era of increasing myeloid cell diversity. *Nat Rev Immunol* **21**, 485-498, doi:10.1038/s41577-020-00490-y (2021).
- 103 Alicea-Torres, K. *et al.* Immune suppressive activity of myeloid-derived suppressor cells in cancer requires inactivation of the type I interferon pathway. *Nat Commun* **12**, 1717, doi:10.1038/s41467-021-22033-2 (2021).
- 104 Lin, J. L. J. *et al.* Oxidative Stress Impairs Cell Death by Repressing the Nuclease Activity of Mitochondrial Endonuclease G. *Cell Rep* **16**, 279-287, doi:10.1016/j.celrep.2016.05.090 (2016).
- 105 Ishihara, Y. & Shimamoto, N. Involvement of endonuclease G in nucleosomal DNA fragmentation under sustained endogenous oxidative stress. *J Biol Chem* **281**, 6726-

- 6733, doi:10.1074/jbc.M510382200 (2006).
- 106 Huang, K. J., Ku, C. C. & Lehman, I. R. Endonuclease G: a role for the enzyme in recombination and cellular proliferation. *Proc Natl Acad Sci U S A* **103**, 8995-9000, doi:10.1073/pnas.0603445103 (2006).
- 107 Wiehe, R. S. *et al.* Endonuclease G promotes mitochondrial genome cleavage and replication. *Oncotarget* **9**, 18309-18326, doi:10.18632/oncotarget.24822 (2018).
- 108 van Loo, G. *et al.* Endonuclease G: a mitochondrial protein released in apoptosis and involved in caspase-independent DNA degradation. *Cell Death Differ* **8**, 1136-1142, doi:10.1038/sj.cdd.4400944 (2001).
- 109 Wang, X., Yang, C., Chai, J., Shi, Y. & Xue, D. Mechanisms of AIF-mediated apoptotic DNA degradation in *Caenorhabditis elegans*. *Science* **298**, 1587-1592, doi:10.1126/science.1076194 (2002).
- 110 Parrish, J. *et al.* Mitochondrial endonuclease G is important for apoptosis in *C-elegans*. *Nature* **412**, 90-94, doi:Doi 10.1038/35083608 (2001).
- 111 Marcotte, R., Lacelle, C. & Wang, E. Senescent fibroblasts resist apoptosis by downregulating caspase-3. *Mech Ageing Dev* **125**, 777-783, doi:10.1016/j.mad.2004.07.007 (2004).
- 112 Kim, J. *et al.* VDAC oligomers form mitochondrial pores to release mtDNA fragments and promote lupus-like disease. *Science* **366**, 1531-1536, doi:10.1126/science.aav4011 (2019).
- 113 Correia-Melo, C. *et al.* Mitochondria are required for pro-ageing features of the senescent phenotype. *EMBO J* **35**, 724-742, doi:10.15252/emj.201592862 (2016).
- 114 Liu, S., Feng, M. & Guan, W. Mitochondrial DNA sensing by STING signaling participates in inflammation, cancer and beyond. *Int J Cancer* **139**, 736-741, doi:10.1002/ijc.30074 (2016).

- 115 Zheng, J. *et al.* Comprehensive elaboration of the cGAS-STING signaling axis in cancer development and immunotherapy. *Mol Cancer* **19**, 133, doi:10.1186/s12943-020-01250-1 (2020).
- 116 Bakhoun, S. F. *et al.* Chromosomal instability drives metastasis through a cytosolic DNA response. *Nature* **553**, 467-472, doi:10.1038/nature25432 (2018).
- 117 Li, S. *et al.* STING-induced regulatory B cells compromise NK function in cancer immunity. *Nature* **610**, 373-380, doi:10.1038/s41586-022-05254-3 (2022).
- 118 Sun, Y. *et al.* The downregulation of type I IFN signaling in G-MDSCs under tumor conditions promotes their development towards an immunosuppressive phenotype. *Cell Death Dis* **13**, 36, doi:10.1038/s41419-021-04487-w (2022).
- 119 Rongvaux, A. *et al.* Apoptotic caspases prevent the induction of type I interferons by mitochondrial DNA. *Cell* **159**, 1563-1577, doi:10.1016/j.cell.2014.11.037 (2014).